

1 An updated synthesis of ocean total alkalinity and dissolved inorganic carbon measurements  
2 from 1993 to 2023: the SNAPO-CO2-v2 dataset

3  
4 Nicolas Metzl<sup>1</sup>, Jonathan Fin<sup>1,2,3</sup>, Claire Lo Monaco<sup>1</sup>, Claude Mignon<sup>1</sup>, Samir Alliouane<sup>4</sup>, Bruno Bombled<sup>5</sup>,  
5 Jacqueline Boutin<sup>1</sup>, Yann Bozec<sup>6</sup>, Steeve Comeau<sup>4</sup>, Pascal Conan<sup>7,8</sup>, Laurent Coppola<sup>4,8</sup>, Pascale Cuet<sup>9</sup>, Eva  
6 Ferreira<sup>5</sup>, Jean-Pierre Gattuso<sup>4,10</sup>, Frédéric Gazeau<sup>4</sup>, Catherine Goyet<sup>11</sup>, Emilie Grossteffan<sup>12</sup>, Bruno Lansard<sup>5</sup>,  
7 Dominique Lefèvre<sup>13</sup>, Nathalie Lefèvre<sup>1</sup>, Coraline Leseurre<sup>14</sup>, Sébastien Petton<sup>15</sup>, Mireille Pujo-Pay<sup>8</sup>, Christophe  
8 Rabouille<sup>5</sup>, Gilles Reverdin<sup>1</sup>, Céline Ridame<sup>1</sup>, Peggy Rimmelin-Maury<sup>12</sup>, Jean-François Ternon<sup>16</sup>, Franck  
9 Touratier<sup>11</sup>, Aline Tribollet<sup>1</sup>, Thibaut Wagener<sup>13</sup>, Cathy Wimart-Rousseau<sup>17</sup>.

10  
11 <sup>1</sup> Laboratoire LOCEAN/IPSL, Sorbonne Université-CNRS-IRD-MNHN, Paris, 75005, France

12 <sup>2</sup> OSU Ecce Terra, Sorbonne Université-CNRS, Paris, 75005, France

13 <sup>3</sup> Now at Institut des Sciences de la Terre, Grenoble, 38058, France

14 <sup>4</sup> Sorbonne Université, CNRS, Laboratoire d'Océanographie de Villefranche, LOV, F-06230 Villefranche-sur-  
15 Mer, France

16 <sup>5</sup> Laboratoire des Sciences du Climat et de l'Environnement, LSCE/IPSL, UMR 8212 CEA- CNRS-UVSQ,  
17 Université Paris-Saclay, 91191 Gif-sur-Yvette, France

18 <sup>6</sup> Station Biologique de Roscoff, UMR 7144 – EDYCO-CHIMAR, Roscoff, France

19 <sup>7</sup> Sorbonne Université, CNRS, Laboratoire d'Océanographie Microbienne, LOMIC, F-66650 Banyuls-sur-Mer,  
20 France

21 <sup>8</sup> Sorbonne Université, CNRS OSU STAMAR - UAR2017, 4 Place Jussieu, 75252, Paris cedex 05, France

22 <sup>9</sup> Laboratoire ENTROPIE and Laboratoire d'Excellence CORAIL, Université de La Réunion-IRD- CNRS-  
23 IFREMER-Université de la Nouvelle-Calédonie, 97744, Saint-Denis, La Réunion, France

24 <sup>10</sup> Institute for Sustainable Development and International Relations, Sciences Po, 27 rue Saint Guillaume, F-  
25 75007 Paris, France

26 <sup>11</sup> Espace-Dev UMR 228 Université de Perpignan Via Domitia, IRD, UM, UA, UG, 66860, Perpignan, France

27 <sup>12</sup> Institut Universitaire Européen de la Mer (OSU-IUEM), Univ Brest, CNRS-UAR3113, 29280, Plouzané,  
28 France

29 <sup>13</sup> Aix Marseille Univ, Université de Toulon, CNRS, IRD, MIO, Marseille, France

30 <sup>14</sup> Flanders Marine Institute (VLIZ), 8400 Ostend, Belgium

31 <sup>15</sup> Ifremer, Univ Brest, CNRS, IRD, LEMAR, F-29840 Argenton, France

32 <sup>16</sup> MARBEC, Univ Montpellier, CNRS, Ifremer, IRD, Sète, France

33 <sup>17</sup> National Oceanography Centre Southampton, European Way, Southampton, SO14 3ZH, UK

34  
35 *Correspondence to:* Nicolas Metzl (nicolas.metzl@locean.ipsl.fr)  
36

37 **Abstract.** Total alkalinity ( $A_T$ ) and dissolved inorganic carbon ( $C_T$ ) in the oceans are important properties to  
38 understand the ocean carbon cycle and its link with global change (ocean carbon sinks and sources, ocean  
39 acidification) and ultimately find carbon based solutions or mitigation procedures (marine carbon removal). We  
40 present an extended database (SNAPO-CO2, Metzl et al, 2024d) with 24700 new additional data for the period  
41 2002 to 2023. The full database now includes more than 67000  $A_T$  and  $C_T$  observations along with basic  
42 ancillary data (time and space location, depth, temperature and salinity) in various oceanic regions obtained since  
43 1993 mainly in the frame of French research projects. This includes both surface and water columns data  
44 acquired in open oceans, coastal zones, rivers and in the Mediterranean Sea and either from time-series or  
45 punctual cruises. Most  $A_T$  and  $C_T$  data in this synthesis were measured from discrete samples using the same  
46 closed-cell potentiometric titration calibrated with Certified Reference Material, with an overall accuracy of  $\pm 4$   
47  $\mu\text{mol kg}^{-1}$  for both  $A_T$  and  $C_T$ . The same technique was used onboard for underway measurements during cruises  
48 conducted in the Southern Indian and Southern Oceans. The  $A_T$  and  $C_T$  data from these cruises are also added in

49 this synthesis. The data are provided in one dataset for the global ocean (<https://doi.org/10.17882/102337>) that  
50 offers a direct use for regional or global purposes, e.g.  $A_T$ /Salinity relationships, long-term  $C_T$  estimates,  
51 constraint and validation of diagnostics  $C_T$  and  $A_T$  reconstructed fields or ocean carbon and coupled  
52 climate/carbon models simulations, as well as data derived from Biogeochemical-Argo (BGC-Argo) floats.  
53 These data can also be used to calculate pH, fugacity of  $\text{CO}_2$  ( $f\text{CO}_2$ ) and other carbon system properties to derive  
54 ocean acidification rates or air-sea  $\text{CO}_2$  fluxes.

55

## 56 **1 Introduction**

57

58 The ocean plays a major role in reducing the impact of climate change by absorbing more than 90% of  
59 the excess heat in the climate system (Cheng et al., 2020, 2024; von Schuckmann et al, 2023; IPCC, 2022) and  
60 about 25% of human released  $\text{CO}_2$  (Friedlingstein et al., 2022, 2023). In the last decade, the oceans experienced  
61 a rapid warming, the year 2023 being the hottest since 1955 (Cheng et al, 2024). In the atmosphere the  $\text{CO}_2$   
62 concentration continues its terrific progressive rising, reaching 419.3 ppm in 2023 (a rate of +2.83 ppm yr<sup>-1</sup>, Lan  
63 et al 2024). In August 2024, the global atmospheric  $\text{CO}_2$  concentration was already above 420 ppm. In the next  
64 decade the oceans will continue to capture heat and  $\text{CO}_2$ , somehow limiting the climate change, but this oceanic  
65  $\text{CO}_2$  uptake changes the chemistry of seawater reducing its buffering capacity (Revelle and Suess, 1957; Jiang et  
66 al, 2023). This process known as ocean acidification has potential impacts on marine organisms (Fabry et al.,  
67 2008; Doney et al., 2009, 2020; Gattuso et al., 2015). With atmospheric  $\text{CO}_2$  concentrations, surface ocean  
68 temperature and ocean heat content, sea-level, sea-ice and glaciers, the ocean acidification (decrease of pH) is  
69 now recognized by the World Meteorological Organization as one of the 7 key properties for global climate  
70 indicators (WMO, 2018). Ocean acidification is specifically referred in the SDG indicator 14.3.1 coordinated at  
71 the Intergovernmental Oceanographic Commission (IOC) of UNESCO. Observing the carbonate system in the  
72 open oceans, coastal zones and marginal seas and understanding how this system changes over time is thus  
73 highly relevant not only to quantify the global ocean carbon budget, the anthropogenic  $\text{CO}_2$  inventories or ocean  
74 acidification rates, but also to understand and simulate the processes that govern the complex  $\text{CO}_2$  cycle in the  
75 ocean (e.g. Goyet et al, 2016, 2019) and to better predict the future evolution of climate and global changes  
76 (Eyring et al., 2016; Kwiatkowski et al., 2020; Jiang et al., 2023). As the rate of change in ocean acidification  
77 presents large temporal and regional variability, long-term observations are required. Weekly to monthly regular  
78 resolution data are needed to better investigate the long-term change of the carbonate system in regions subject  
79 to extreme events (e.g. tropical cyclones, marine heat or cold waves, rapid freshening, convection, dust events,  
80 river discharges, etc....). In this context it is recommended to progress in data synthesis of the ocean carbon  
81 observations that would offer new high quality products for the community (e.g. for GOA-ON, [www.goa-on.org](http://www.goa-on.org),  
82 IOC/SDG 14.1.3, <https://oa.iode.org/>, Tilbrook et al., 2019).

83 In this work, following the first SNAPO- $\text{CO}_2$  synthesis product (Metzl et al, 2024a), we present a new  
84 synthesis of more than 67000  $A_T$  and  $C_T$  data, measured either on shore or onboard Research Vessels obtained  
85 over the 1993-2023 period during various cruises or at time-series stations mainly supported by French projects.  
86 Hereafter this new dataset will be cited as SNAPO- $\text{CO}_2$ -v2. The methods, data assemblage and quality control  
87 were presented in version V1. Here, we describe the new data added and discuss some potential uses of this  
88 dataset.

89

## 90 2 Data collections

91

92 The time series projects and research cruises from which new data were collated are listed in Table 1  
93 with information and references in the Supplementary file (Tables S1, S3 and S4). The sampling locations of  
94 new data are displayed in Figure 1 (the location for all data presented in Figure S1). Sampling was performed  
95 either from CTD-Rosette casts (Niskin bottles) or from the ship's seawater supply (intake at about 5m depth  
96 depending on the ship and swell). Samples collected in 500 mL borosilicate glass bottles were poisoned with 100  
97 to 300  $\mu\text{L}$  of  $\text{HgCl}_2$  depending on the cruises, closed with greased stoppers (Apiezon®) and held tight using  
98 elastic band following the SOP protocol (DOE, 1994; Dickson et al., 2007). Some samples were also collected in  
99 500 mL bottles closed with screw caps. After completion of each cruise, most of discrete samples were returned  
100 back to the LOCEAN laboratory (Paris, France) and stored in a dark room at 4 °C before analysis generally  
101 within 2-3 months after sampling (sometimes within a week). In this version we added data from samples that  
102 were also returned to University of Perpignan or to University of La Réunion. In addition to discrete samples  
103 analyzed for various projects conducted mainly in the North Atlantic, Tropical Atlantic, Mediterranean Sea and  
104 coastal regions (Table 1), we complemented this second synthesis with  $A_T$  and  $C_T$  surface observations obtained  
105 in the Indian and Southern oceans during the OISO cruises in 2019-2021 (Leseurre et al., 2022; Metzl et al,  
106 2022; data also available at NCEI/OCADS: [www.nodc.noaa.gov/ocads/oceans/VOS\\_Program/OISO.html](http://www.nodc.noaa.gov/ocads/oceans/VOS_Program/OISO.html)) and  
107 MINERVE cruises in 2002-2018 (Laika et al, 2009; Brandon et al, 2022). The  $A_T$  and  $C_T$  measurements from the  
108 MINERVE cruises were performed either onboard R/V Astrolabe or back in the laboratories (at LOCEAN  
109 laboratory and at University of Perpignan).

110

111

112

113

114

115

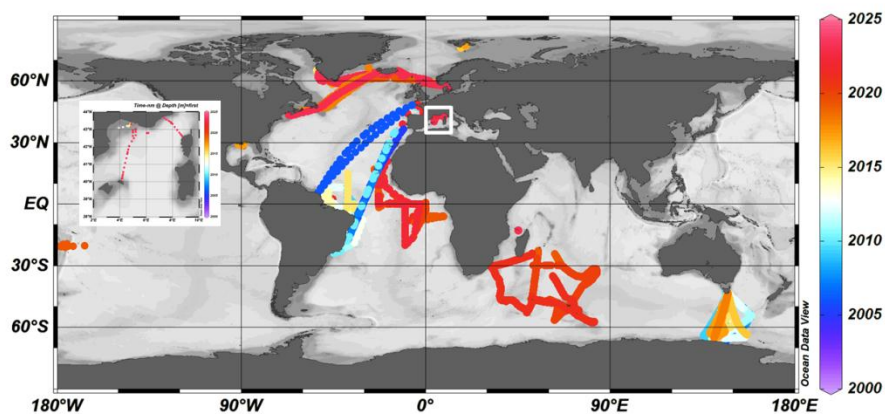
116

117

118

119

120



121 **Figure 1:** Locations of new  $A_T$  and  $C_T$  data (2005-2023) in the Global Ocean and the Western Mediterranean Sea  
122 (white box, insert) in the SNAPO-CO2-v2 dataset. Color code is for Year. Figure produced with ODV (Schlitzer,  
123 2018).

124

125 **Table 1:** List of cruises added in the SNAPO-CO<sub>2</sub>-v2 dataset. This is organized by region from North to South  
 126 and the Mediterranean Sea. See Tables S1, S2, S3 and S4 in the Supplementary Material for a list of laboratories,  
 127 of CRMs used, for DOI and for references of cruises. Nb = the number of data for each cruise or time-series. \*  
 128 indicates the measurements at sea (surface underway).

Cruise/Project	Start	End	Region	Sampling	Nb	
134	STEP	2016	2017	Arctic	Water Column	33
135	SURATLANT AX1	2017	2023	North Atlantic	Surface	255
136	SURATLANT AX2	2018	2023	North Atlantic	Surface	224
137	VOS	2005	2010	Atlantic	Surface	192
138	MISSRHODIA-1	2017	2017	Gulf Mexico	Water Column	8
139	ACIDHYPO	2022	2022	Gulf Mexico	Water Column	10
140	CAMFIN-WATL	2010	2015	Trop Atlantic	Surface	192
141	PIRATA-BR	2009	2015	Trop Atlantic	Surface	194
142	BIOAMAZON	2013	2014	Trop Atlantic	Surface	62
143	AMAZOMIX	2021	2021	Trop Atlantic	Water Column	180
144	PIRATA-FR	2019	2019	Trop Atlantic	Surface	93
145	PIRATA-FR	2020	2020	Trop Atlantic	Surface, Water Column	58
146	PIRATA-FR	2021	2021	Trop Atlantic	Surface, Water Column	79
147	PIRATA-FR	2022	2022	Trop Atlantic	Surface, Water Column	118
148	CO2ARVOR	2009	2010	Atlantic, Coastal	Surface, Water Column	621
149	SOMLIT-Roscoff	2020	2022	Coastal North Atl	Surface and 60m	207
150	SOMLIT-Brest	2020	2022	Coastal North Atl	Surface	251
151	TONGA	2019	2019	Trop Pacific	Water Column	226
152	CARBODISS	2018	2019	Indian Mayotte	Surface	85
153	OISO *	2019	2021	South Indian	Surface	5258
154	MINERVE	2004	2018	Southern Ocean	Surface	1077
155	MINERVE *	2002	2013	Southern Ocean	Surface	11258
156	COCORICO2	2017	2022	Coastal	Surface	589
157	SOMLIT-PointB	2019	2023	MedSea Coastal	Surface and 50m	716
158	SOLEMIO	2018	2022	MedSea Coastal	Water Column	271
159	ANTARES	2017	2023	MedSea	Water Column	506
160	MOLA	2018	2023	MedSea Coastal	Water Column	193
161	DYFAMED	2018	2023	MedSea	Water Column	514
162	MESURHO-BENT	2010	2011	MedSea Coastal	Surface and sub-surface	25
163	ACCESS-01	2012	2012	MedSea Coastal	Water Column	16
164	CARBO-DELTA-2	2013	2013	MedSea Coastal	Water Column	14
165	DICASE	2014	2014	MedSea Coastal	Water Column	22
166	MISSRHODIA-2	2018	2018	MedSea Coastal	Surface and sub-surface	13
167	DELTARHONE1	2022	2022	MedSea Coastal	Water Column	9
168	MOOSE-GE	2021	2021	MedSea	Water Column	451
169	MOOSE-GE	2022	2022	MedSea	Water Column	447
170	MOOSE-GE	2023	2023	MedSea	Water Column	475

171  
172

### 173 3 Method, accuracy, repeatability and quality control

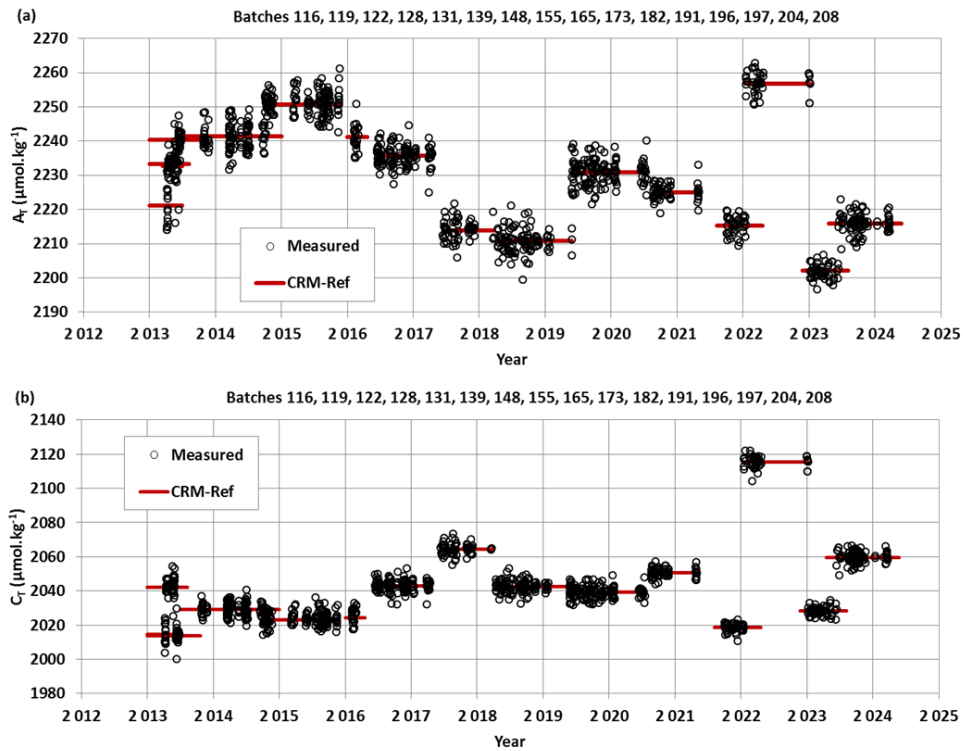
174

#### 175 3.1 Method and accuracy

176

177 Since 2003, the discrete samples returned back at SNAPO-CO<sub>2</sub> Service facilities (LOCEAN, Paris),  
 178 were analyzed simultaneously for A<sub>T</sub> and C<sub>T</sub> by potentiometric titration using a closed cell (Edmond, 1970;  
 179 Goyet et al., 1991). The same technique was used at sea for surface water underway measurements during OISO  
 180 and MINERVE cruises (indicated by \* in Table 1). In the late 1980s the so-called “JGOFS-IOC Advisory Panel  
 181 on Ocean CO<sub>2</sub>” recommended the need for standard analysis protocols and for developing Certified Reference  
 182 Materials (CRMs) for inorganic carbon measurements (Poisson et al., 1990; UNESCO, 1990, 1991). The CRMs

183 were provided to international laboratories by Pr. A. Dickson (Scripps Institution of Oceanography, San Diego,  
 184 USA), starting in 1990 for  $C_T$  and 1996 for  $A_T$ , respectively. These CRMs were thus always available to us and  
 185 used to calibrate the measurements (CRM Batch numbers used for each cruise are listed in the Supplementary  
 186 file, Table S2). The CRMs accuracy, as indicated in the certificate for each Batch, is around  $\pm 0.5 \mu\text{mol kg}^{-1}$  for  
 187 both  $A_T$  and  $C_T$  ([www.nodc.noaa.gov/ocads/oceans/Dickson\\_CRM/batches.html](http://www.nodc.noaa.gov/ocads/oceans/Dickson_CRM/batches.html)). The concentrations of CRMs  
 188 we used vary between 2193 and 2426  $\mu\text{mol kg}^{-1}$  for  $A_T$  and between 1968 and 2115  $\mu\text{mol kg}^{-1}$  for  $C_T$   
 189 corresponding to the range of concentrations observed in open ocean water. In the Mediterranean Sea the  
 190 concentrations are higher ( $A_T > 2600 \mu\text{mol kg}^{-1}$  and  $C_T > 2300 \mu\text{mol kg}^{-1}$ ) and in the coastal zones or near the  
 191 Amazon River plume the concentrations were often lower than the CRMs ( $A_T < 1500 \mu\text{mol kg}^{-1}$  and  $C_T < 1000$   
 192  $\mu\text{mol kg}^{-1}$ ). Results of analyses performed on 1242 CRM bottles (different Batches) in 2013-2024 are presented  
 193 in Figure 2. The standard-deviations (Std) of the differences of measurements were on average  $\pm 2.69 \mu\text{mol kg}^{-1}$   
 194 for  $A_T$  and  $\pm 2.88 \mu\text{mol kg}^{-1}$  for  $C_T$ . For unknown reasons, the differences were occasionally up to 10-15  $\mu\text{mol kg}^{-1}$   
 195 <sup>1</sup> (1.2% of the data, Figure S2). These few CRM measurements were discarded for the data processing. We did  
 196 not detect any specific signal for CRM analyses (e.g., larger uncertainty depending on the Batch number or  
 197 temporal drifts during analyses, Figure 2) but for some cruises the accuracy based on CRMs could be better than  
 198 3  $\mu\text{mol kg}^{-1}$  (e.g.  $< 3 \mu\text{mol kg}^{-1}$  for AMAZOMIX cruise using 6 Batches #197 and for MOOSE-GE 2022 using  
 199 19 Batches #204, or  $< 1.5 \mu\text{mol kg}^{-1}$  for SOMLIT-Point-B in 2022 using 6 Batches #204).



220 **Figure 2:**  $A_T$  (a) and  $C_T$  (b) analyses for different CRM Batches measured in 2013-2024. For these 1242  
 221 analyses the mean and standard-deviations of the differences with the CRM reference were  $-0.11 (\pm 2.69) \mu\text{mol}$   
 222  $\text{kg}^{-1}$  for  $A_T$  and  $0.01 (\pm 2.88) \mu\text{mol kg}^{-1}$  for  $C_T$ .

### 226 3.2 Repeatability

227

228 For some projects, duplicates have been regularly sampled (SOMLIT-Point-B, SOMLIT-Brest) or  
229 replicate bottles sampled at selected depths at fixed stations during the cruises (e.g. STEP, CARBODISS). In the  
230 first synthesis of the SNAPO-CO<sub>2</sub> dataset we showed the results from several time-series (SOMLIT-Point-B,  
231 SOMLIT-Brest and BOUSSOLE/DYFAMED). Here we present the results for the new data obtained at  
232 SOMLIT-Point-B in the coastal Mediterranean Sea and SOMLIT-Brest in the Bay of Brest (Figure 3). Results of  
233  $A_T$  and  $C_T$  repeatability are synthesized in Table 2. For the OISO cruises conducted in 2019, 2020 and 2021 the  
234 repeatability was evaluated from duplicate analyses (within 20 minutes time) of continuous sea surface  
235 underway sampling at the same location (when the ship was stopped). Similarly to what was found for the CRM  
236 measurements (Figure S2), differences in duplicates are occasionally higher than 10-15  $\mu\text{mol kg}^{-1}$  (Figure 3) but  
237 most of the duplicates for all projects are within 0 to 3  $\mu\text{mol kg}^{-1}$ . Compared to previous results (Kapsenberg et  
238 al. 2017; Metzl et al, 2024a), there are larger differences between duplicates at SOMLIT-B in 2019-2023 (up to  
239 30  $\mu\text{mol kg}^{-1}$ , Figure 3) leading to relatively large Std around 5 and 6  $\mu\text{mol kg}^{-1}$  for both  $A_T$  and  $C_T$  (Table 2).  
240 The same was observed for duplicates at SOMLIT-Brest (Table 2). We do have not yet a clear explanation for  
241 this large Std although larger variability was observed in recent years, and the measurements were performed  
242 later after the sampling (e.g. more than 6 months for some samples during and after the COVID period). We will  
243 see that given the temporal variability of the properties this does not lead to suspicious interpretation for the  
244 seasonality or the trend analyses of these time-series.

245

246

247

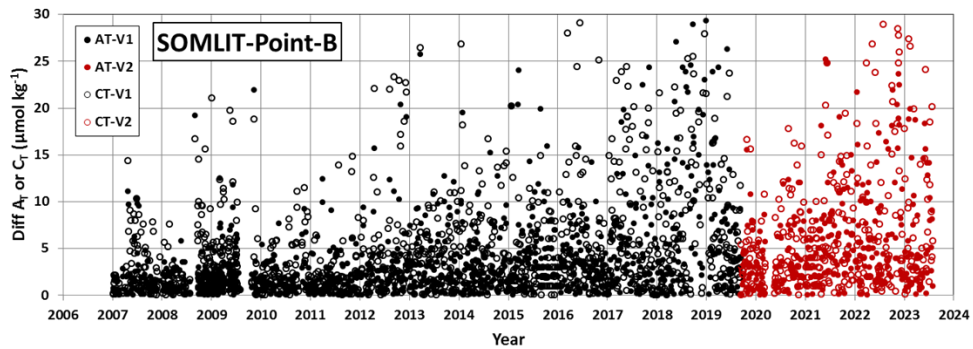
248

249

250

251

252



252

253

254

255

256

257

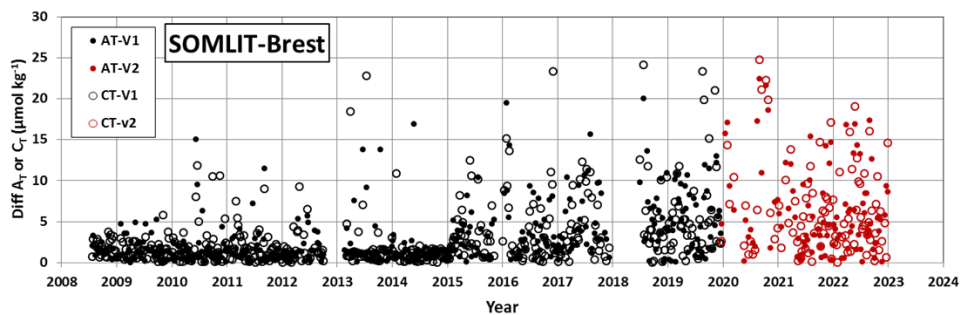
258

259

260

261

262



263 **Figure 3:** Results of duplicate  $A_T$  and  $C_T$  analyses from the time-series SOMLIT-Point-B in the coastal  
264 Mediterranean Sea and SOMLIT-Brest in the coastal Brittany for the data in the SNAPO-CO<sub>2</sub>-v1 dataset (black)  
265 and new data added in SNAPO-CO<sub>2</sub>-v2 (red). The plots show differences in duplicates for both  $A_T$  (filled  
266 circles) and  $C_T$  (open circles). Standard-deviations of these duplicates are listed in Table 2.

267

268

269 **Table 2:** Repeatability of  $A_T$  and  $C_T$  analyses for cruises with duplicate analysis. The results are expressed as the  
 270 standard-deviations (Std) of the analysis of replicated samples. Nb = the number of replicates for each Time-  
 271 series or Cruise. For the OISO cruises the mean repeatability was obtained from measurements at the same  
 272 location (when the ship stopped).

Cruise	Period	Nb	Std $A_T$ $\mu\text{mol kg}^{-1}$	Std $C_T$ $\mu\text{mol kg}^{-1}$	Reference
STEP	2017	3	0.7	2.8	Unpublished
CARBODISS	2018	10	6.72	5.71	Unpublished
SOMLIT-Point-B	2007-2019	1130	4.5	5.1	SNAPO-CO2-v1, (a)
SOMLIT-Point-B	2019-2023	321	5.2	6.2	SNAPO-CO2-v2, (a)
SOMLIT-Brest	2008-2018	404	3.1	3.4	SNAPO-CO2-v1, (a)
SOMLIT-Brest	2019-2022	142	6.0	6.1	SNAPO-CO2-v2, (a)
OISO 29	2019	46	1.8	1.8	Leseurre et al (2022), (b)
OISO 30	2020	67	1.5	2.0	Metzl et al. (2022), (b)
OISO 31	2021	343	2.6	3.3	Metzl et al (2024c), (b)

292 (a) See Figure 3 for the results of regular duplicates for time-series SOMLIT-Point-B, SOMLIT-Brest.

293 (b) Metadata and data available at [www.nodc.noaa.gov/ocads/oceans/VOS\\_Program/OISO.html](http://www.nodc.noaa.gov/ocads/oceans/VOS_Program/OISO.html)

### 295 3.3 Assigned flags for quality control

296  
 297 Identifying each data with an appropriate flag is very convenient for selecting the data (good,  
 298 questionable or bad). Here we used 4 flags for each property (flags 2 = good, 3= questionable, 4=bad, and 9= no  
 299 data) following the WOCE program and used in other data products such as SOCAT (Bakker et al., 2016) or  
 300 GLODAP (Olsen et al., 2016; Lauvset et al., 2024). During the data-processing, we first assigned a flag for each  
 301  $A_T$  and  $C_T$  data based on the standard error in the calculation of  $A_T$  and  $C_T$  concentrations (non-linear regression,  
 302 Dickson et al. 2007). By default, if the standard deviation on the regression is  $> 1 \mu\text{mol kg}^{-1}$ , we assigned a flag 3  
 303 (questionable) although the data could be acceptable and then used for interpretations. Flag 3 was also assigned  
 304 when salinity was doubtful or when differences of duplicates were large (e.g.  $\pm 20 \mu\text{mol kg}^{-1}$ ). Flags 4 (bad or  
 305 certainly bad) were assigned when clear anomalies were detected for unknown reasons (e.g. a sample probably  
 306 not fixed with  $\text{HgCl}_2$  or analysis performed late during the COVID issue). A secondary quality control was  
 307 performed by the PIs of each project based on data inspection, duplicates,  $A_T$ /Salinity relationship, or the mean  
 308 observations in deep layers where large variability in  $A_T$  and  $C_T$  is unlikely to occur from year to year.

309 An example for quality flag is presented for all data from the MINERVE cruises conducted in 2002-  
 310 2018 in the Southern Ocean where clear outliers have been identified (Figure S3). For the MINERVE cruises in  
 311 2002-2018 and a total of 12335  $A_T$  and  $C_T$  analyses, 24 were identified as bad (flag 4), 978 for  $A_T$  and 971 for  $C_T$   
 312 listed as questionable (flag 3), and all others are considered as good data (flag 2, i.e. about 92%). For the  
 313 MOOSE-GE cruises in 2021, 2022 and 2023 (new data in SNAPO-CO2-v2) and a total of 1373  $A_T$  and  $C_T$   
 314 analyses, 2 were identified flagged as bad (flag 4), 38 for  $A_T$  and 33 for  $C_T$  listed as questionable (flag 3) all  
 315 others were considered as good data (flag 2, i.e. 97%). This is better than the statistics we evaluated for the  
 316 SNAPO-CO2-v1 dataset (90% flag 2 for MOOSE-GE in 2010-2019). A similar control was performed for each  
 317 project.

### 318 **3.4 Inter-comparisons**

319

320 Inter-comparisons of measurements performed for different cruises or with different techniques help to  
321 evaluate the quality of the data and detect potential biases when merging the data in the same region obtained by  
322 different laboratories at different periods. This is especially important to interpret long-term trends of  $A_T$  and  $C_T$   
323 as well as for  $p\text{CO}_2$  and pH calculated with  $A_T$   $C_T$  pairs. The synthesis of various cruises in the same region and  
324 periods also offers verification and secondary control of the data.

325

#### 326 **3.4.1 Comparisons in deep layers**

327

328 Comparisons of data in the deep layers from different cruises are useful for secondary quality control as  
329 one expects low natural variability or anthropogenic signals from season to season and over a few years. Several  
330 cruises were conducted in the Mediterranean Sea in 2017-2023 (MOOSE-GE, ANTARES and DYFAMED). The  
331 mean values of  $C_T$  and  $A_T$  in the deep layers ( $> 1800\text{m}$ ) for each cruise confirmed the coherence of the data  
332 (Table 4). The  $C_T$  and  $A_T$  concentrations are also in the range of the mean values evaluated for cruises conducted  
333 in 2014 in the Mediterranean Sea (results listed in the SNAPO-CO<sub>2</sub>-v1 synthesis, Metzl et al, 2024a). In the  
334 western tropical Pacific we also observed coherent properties for the TONGA and OUTPACE cruises (Wagener  
335 et al, 2018) for data selected at 1800-2300m layer corresponding to the  $C_T$  maximum layer in the Pacific Deep  
336 Water (PDW). On the other hand in the western tropical Atlantic near the Amazon River plume where the spatial  
337 variability of the properties is large at the surface (Ternon et al, 2000; Mu et al, 2021; Olivier et al, 2022) the  
338 comparison in the water column is less clear (Figure S4). Nevertheless for the AMAZOMIX and the TARA-  
339 Microbiome cruises, both conducted in September 2021, the results at close stations (around 5°N/50°W) suggest  
340 very similar concentrations at 1000m (Table 4). The comparisons in deep waters enabled to merge the different  
341 datasets for interpretations of the temporal trends and processes driving the CO<sub>2</sub> cycle in these regions (e. g.  
342 Ulses et al., 2023 and Wimart-Rousseau et al., 2023 for the Mediterranean Sea)

343

#### 344 **3.4.2 Comparing on board and on shore results**

345

346 In surface waters where the variability is high inter-comparison is not relevant for secondary quality  
347 control. However, during the MINERVE cruises, discrete samples were occasionally performed along with sea  
348 surface underway measurements. Thus, we can compare  $A_T$  and  $C_T$  measured in the laboratory with those  
349 measured onboard as described by Laika et al. (2009) for the MINERVE cruises in 2005-2006. It should be  
350 noticed that the discrete samples were measured after a long trip (shipping boxes from Hobart, Tasmania to  
351 Paris, France) and thus generally analyzed at least 3 months after the cruises (cruises conducted in October to  
352 February, analyses performed in May-June). Given all the uncertainties associated to the sampling, samples  
353 storage and transport, analyses and CRMs, the mean differences between discrete and underway data are still  
354 reasonable (Std ranging between 4 and 12  $\mu\text{mol kg}^{-1}$ , Table 5). For unknown reasons the mean difference was  
355 high for a cruise in 2008-2009 (Std  $> 10 \mu\text{mol kg}^{-1}$ , the “weather goal”, Newton et al., 2015). With this in mind,  
356 we believe the MINERVE data (both underway and discrete data) are useful to interpret the change of properties  
357 in this region at seasonal or decadal scales (Laika et al., 2009; Brandon et al., 2022).

358



359 **Table 4:** Mean observations in the deep layers (> 1800m) of the Ligurian Sea (Western Mediterranean Sea for  
360 different cruises conducted in 2017-2023), of the Tropical Pacific (around 2000m for cruises in 2017 and 2019),  
361 and of the Tropical Atlantic (around 1000m for cruises in 2021).  $N-A_T$  and  $N-C_T$  are  $A_T$  and  $C_T$  normalized at  
362 salinity ( $S = 38$  in the Ligurian Sea;  $S = 35$  for the Pacific and the Atlantic Oceans). Nb = number of data (with  
363 flag 2). Standard deviations are in brackets.

Cruise	Period	Nb	Pot. Temp (°C)	Salinity	$N-A_T$ ( $\mu\text{mol kg}^{-1}$ )	$N-C_T$ ( $\mu\text{mol kg}^{-1}$ )
Ligurian Sea (> 1800m)						
All Cruises	2017-2023	227	12.923 (0.052)	38.484 (0.003)	2558.3 (10.5)	2300.0 (10.7)
DYFAMED	2017-2022	74	12.913 (0.006)	38.485 (0.002)	2555.1 (11.8)	2297.3 (12.4)
ANTARES	2017-2023	62	12.944 (0.096)	38.485 (0.005)	2559.8 (9.0)	2302.2 (8.9)
MOOSE-GE	2017-2023	91	12.917 (0.005)	38.484 (0.003)	2559.8 (9.8)	2300.7 (10.0)
Tropical Pacific (layer 1800-2300m)						
OUTPACE	2017	15	2.124 (0.055)	34.633 (0.006)	2414.1 (8.0)	2318.8 (5.8)
TONGA	2019	7	2.196 (0.197)	34.619 (0.016)	2408.9 (9.1)	2327.2 (7.5)
Western Tropical Atlantic (1000m)						
AMAZOMIX	2021	14	4.770 (0.105)	34.711 (0.041)	2315.6 (20.2)	2220.8 (17.1)
TARA-MICRO	2021	1	4.852	34.717	2312.9	2231.1

402 **Table 5:** Comparison of  $A_T$  and  $C_T$  analysed on-board and at SNAPO-CO2 facilities for the MINERVE project.  
403 The results are expressed as the standard deviations (Std) of the differences for each cruise. Nb = the number of  
404 co-located samples.

Period	Nb	Std $A_T$ $\mu\text{mol kg}^{-1}$	Std $C_T$ $\mu\text{mol kg}^{-1}$
2004-2005	109	12.85	4.99
2005-2006	45	4.20	6.77
2007-2008	17	10.15	10.62
2008-2009	26	15.80	12.02
2009-2010	22	4.04	5.78
2010-2011	33	9.36	6.83
2012-2013	29	5.43	9.73

### 3.4.3 Comparison based on different techniques

422

423 Another example of comparison is presented for samples obtained in the lagoon of Mayotte Island in  
424 the western Indian Ocean and measured using different techniques. In the frame of the CARBODISS project  
425 seawater was sampled in 2018-2023 at several coral reef sites within the north-eastern part of the lagoon and  
426 measured either at LOCEAN laboratory or at La Réunion University. To remove coral sand particles the water  
427 samples were immediately filtered through Whatman GF/F filters and poisoned with mercuric chloride,  
428 following Dickson et al. (2007). In 2021, 2022 and 2023,  $A_T$  was measured at La Réunion University using an  
429 automated potentiometric titration (905 Titrandro Metrohm titrator with combined pH electrode 6.0253.00) and  
430 calculated from the second inflection point of the titration curve. The HCl concentration was checked each day  
431 of measurements using a CRM provided by A. Dickson, Scripps Institution of Oceanography. The  $A_T$  precision  
432 of  $\pm 2 \mu\text{mol kg}^{-1}$  was based on triplicate analyses (Lagoutte et al., 2023). In the studied coral reef sites  $A_T$   
433 concentrations ranged between 2250 and 2350  $\mu\text{mol kg}^{-1}$  but with occasional higher concentrations up to 2450-  
434 2500  $\mu\text{mol kg}^{-1}$ . Such high  $A_T$  has been observed in other coral reefs ecosystems (Cyronak et al., 2013 at Cook  
435 Island; Palacio-Castro et al., 2023 at Middle Keys, Florida). The data obtained in the lagoon of Mayotte on  
436 different coral reefs could be compared with underway observations obtained offshore of Mayotte Island (OISO-  
437 11 cruises in 2004 and CLIM-EPARSES cruise in 2019, data available in the SNAPO-CO2-v1 dataset). In the  
438 open ocean the  $A_T$  concentrations ranged between 2250 and 2330  $\mu\text{mol kg}^{-1}$ , close to the results obtained at  
439 Mayotte reefs except for samples in November 2021 that were all collected at Cratère station (12.84°S-45.39°E)  
440 (Figure 4). At this location there was a large diurnal variation in November 2021 with  $A_T$  increasing from 2322  
441 to 2508  $\mu\text{mol kg}^{-1}$  (Figure S5). This is because in 2021 the samples were taken at low tide recording a volcanic  
442 signal at this site allowing recording for the first time the volcanic signal in this location ( $\text{CO}_2$  resurgences). In  
443 2018 and 2019 such high  $A_T$  were not measured (Figure S5) as samples were taken at high tides allowing a  
444 certain dilution of volcanic  $\text{CO}_2$  emissions in the water column. Although the samples were measured with  
445 different techniques the range of  $A_T$  is coherent for both datasets (Figure 4). Therefore we added the  $A_T$  data  
446 measured at La Réunion University in 2021-2023 to complete the synthesis for this location (Mayotte Island).

447

448

449

450

451

452

453

454

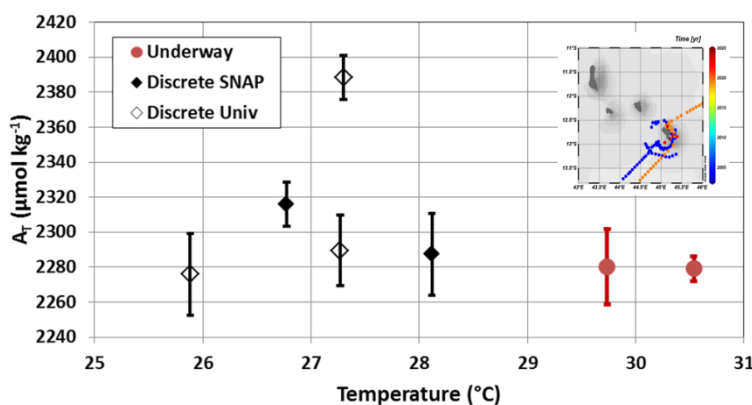
455

456

457

458

459



460 **Figure 4:** Total alkalinity ( $A_T$ ) versus temperature for samples measured around Mayotte and in the coral reef  
461 (insert map). Underway  $A_T$  was measured onboard in 2004 and 2019 (red circles) whereas discrete samples at  
462 different reef sites within the lagoon of Mayotte in 2018, 2019, 2021, 2022 and 2023 were measured at  
463 LOCEAN (black diamonds) or at La Réunion University (open diamonds). The figure presents the data averaged  
464 for each cruise in this region.

465

466 **3.4.4 Summary of quality control data**

467

468 The total number of data in the SNAPO-CO2-v2 dataset for the Global Ocean is gathered in Table 6  
 469 with corresponding flags for each property. Overall, the synthesis includes more than 91% of good data for both  
 470  $A_T$  and  $C_T$ . About 6% are questionable and 3% are likely bad. Overall, we believe that all data (with flag 2) in  
 471 this synthesis have an accuracy better than  $4 \mu\text{mol kg}^{-1}$  for both  $A_T$  and  $C_T$ , the same as for quality-controlled  
 472 data in GLODAP (Lauvset et al., 2024). The uncertainty ranges between the “Climate goal” ( $2 \mu\text{mol kg}^{-1}$ ) and  
 473 the “Weather Goal” ( $10 \mu\text{mol kg}^{-1}$ ) for ocean acidification studies (Newton et al., 2015; Tilbrook et al., 2019).  
 474 This accuracy is also relevant to validate or constraint data-based methods that reconstruct  $A_T$  and  $C_T$  fields with  
 475 an error of around 10-15  $\mu\text{mol kg}^{-1}$  for both properties (Bittig et al., 2018; Broullón et al., 2019, 2020; Fourier et  
 476 al., 2020; Gregor and Gruber, 2021; Chau et al., 2024a).

477

478

479 **Table 6:** Number of Temperature, Salinity,  $A_T$  and  $C_T$  data in the SNAPO-CO2-v2 synthesis identified for flags  
 480 2 (good), 3 (questionable), 4 (bad), 9 (no data). Last column is the percentage of flag 2 (Good).

481

482

Property	Flag 2	Flag 3	Flag 4	Flag 9	% flag 2
Temperature	68253	418	0	653	99.4
Salinity	68706	482	5	131	99.3
$A_T$	61249	3910	2077	2088	91.1
$C_T$	61869	3865	2057	1533	91.3

490

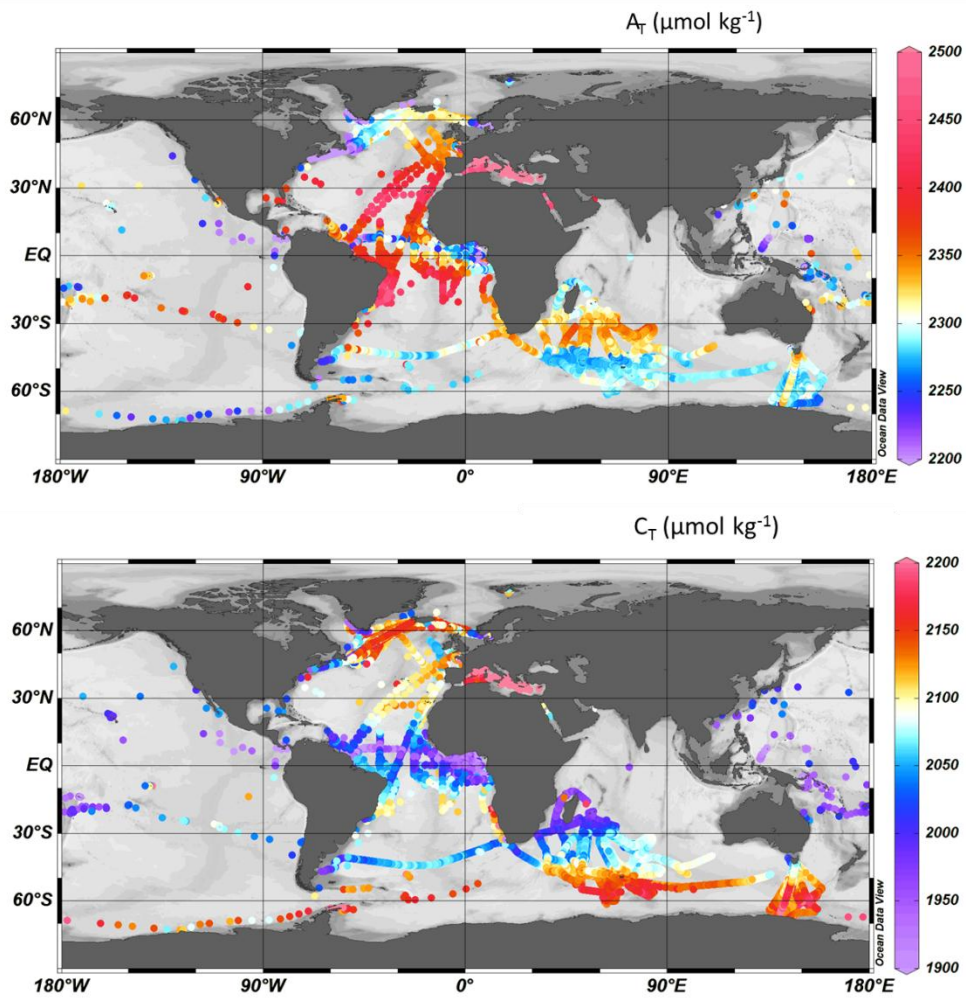
491

492 **4 Global  $A_T$  and  $C_T$  distribution based on the SNAPO-CO2-v2 dataset**

493

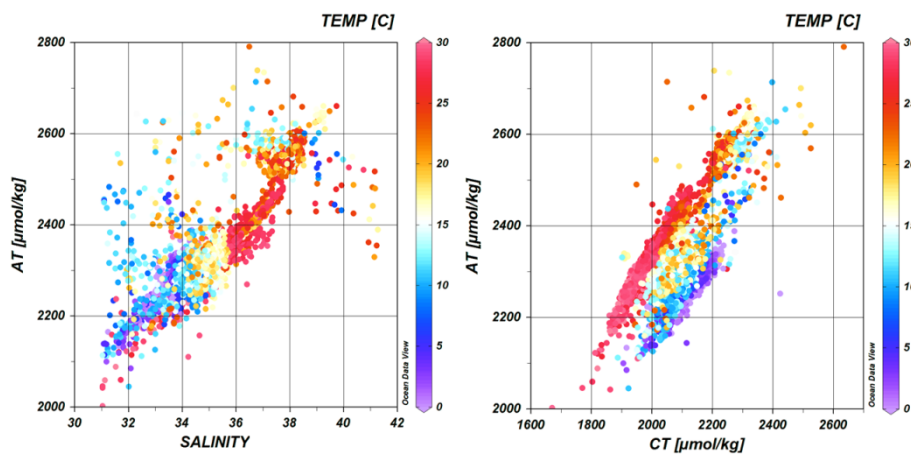
494 The surface distribution in the global ocean based on the SNAPO-CO2 dataset is presented in Figure 5  
 495 for  $A_T$  and  $C_T$ . The  $A_T$ /Salinity and  $A_T$ / $C_T$  relationships are clearly identified and structured at regional scale  
 496 (Figure 6). In the open ocean, high  $A_T$  concentrations ( $> 2400 \mu\text{mol kg}^{-1}$ ) are identified in the Atlantic subtropics  
 497 (bands  $35^\circ\text{N}$ - $15^\circ\text{N}$  and  $25^\circ\text{S}$ - $3^\circ\text{S}$ ) (Jiang et al., 2014; Takahashi et al., 2014). The lowest  $A_T$  and  $C_T$   
 498 concentrations ( $< 600 \mu\text{mol kg}^{-1}$ ) are observed in the western tropical Atlantic in the Amazon River plume near  
 499 the mouth (Lefèvre et al., 2017b). For  $C_T$  the concentrations are high ( $> 2150 \mu\text{mol kg}^{-1}$ ) in the Southern Ocean  
 500 south of the polar front, associated with the deep mixing in winter and the upwelling of deep water (Metzl et al.,  
 501 2006; Pardo et al., 2017). The highest  $C_T$  concentrations (up to  $2180$ - $2270 \mu\text{mol kg}^{-1}$ ) are observed in the high  
 502 latitudes of the Southern Ocean near the Adélie coastal zone (MINERVE and ACE cruises), around the  
 503 Kerguelen plateau (OISO-31 cruise) and close to the Antarctic Peninsula (TARA-Microbiome cruise). In the  
 504 North Atlantic the new data from SURATLANT cruises in 2018-2023 confirm the high  $C_T$  concentrations ( $>$   
 505  $2150 \mu\text{mol kg}^{-1}$ ) observed in the Sub-polar gyre since 2016 due in part to the accumulation of anthropogenic  $\text{CO}_2$   
 506 (Leseurre et al., 2020). Low  $C_T$  concentration ( $< 2000 \mu\text{mol kg}^{-1}$ ) are found in the tropics ( $10^\circ\text{N}$ - $30^\circ\text{S}$ ) with  
 507 lower values ( $< 1950 \mu\text{mol kg}^{-1}$ ) in the equatorial Atlantic band  $10^\circ\text{N}$ -Eq (e.g. Koffi et al., 2010; Lefèvre et al.,  
 508 2021). In the Amazon shelf sector  $C_T$  can reach even lower concentration ( $< 1700 \mu\text{mol kg}^{-1}$ , AMAZOMIX  
 509 cruise).

510  
511  
512  
513  
514  
515  
516  
517  
518  
519  
520  
521  
522  
523  
524  
525  
526  
527  
528  
529  
530  
531  
532  
533  
534  
535  
536  
537  
538



539  
540  
541  
542  
543  
544  
545  
546  
547  
548  
549  
550  
551  
552  
553  
554  
555  
556  
557  
558  
559

**Figure 5:** Distribution of  $A_T$  (top) and  $C_T$  (bottom) concentrations ( $\mu\text{mol.kg}^{-1}$ ) in surface waters (0-10m) in the SNAPO-CO2-v2 dataset. Only data with flag 2 are presented in these figures. Figures produced with ODV (Schlitzer, 2018).



560  
561  
562  
563

**Figure 6:** Relationships between  $A_T$  and Salinity (left panel) and  $A_T$  versus  $C_T$  (right panel) for samples in surface waters (0-10m and Salinity > 31). Only data with flag 2 are presented (nb = 48749). The color scales correspond to the temperature. The data not aligned correspond to coastal zones (e.g. COCORICO2 stations). Figures produced with ODV (Schlitzer, 2018).

564  
565  
566  
567  
568  
569  
570  
571  
572  
573  
574  
575  
576  
577  
578  
579  
580  
581  
582  
583  
584  
585  
586  
587  
588  
589  
590  
591  
592  
593  
594  
595  
596  
597  
598  
599  
600  
601  
602  
603  
604

## 5 Regional $A_T$ and $C_T$ distributions and trends based on the SNAPO-CO2 dataset

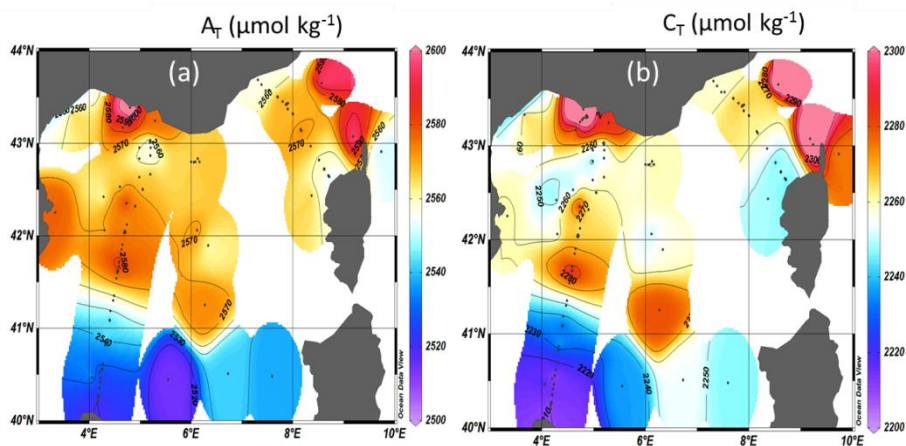
The regional distributions are described for the Mediterranean Sea and for selected regions in the open ocean and coastal zones where the data are available for 10 years or more to explore the  $A_T$  and  $C_T$  trends. Given the observed seasonal and inter-annual variability and that the time-series were not regular (e.g. at monthly frequency), we cannot use recommended methods to estimate the trends (e.g. based on de-seasoned data, Sutton et al, 2022). Here we have selected the locations and seasons where the  $C_T$  trends can be linearly fitted and compared with no interpolation to fill gaps and discontinuous data (e.g., fewer samples during the COVID period).

### 5.1 The Mediterranean Sea

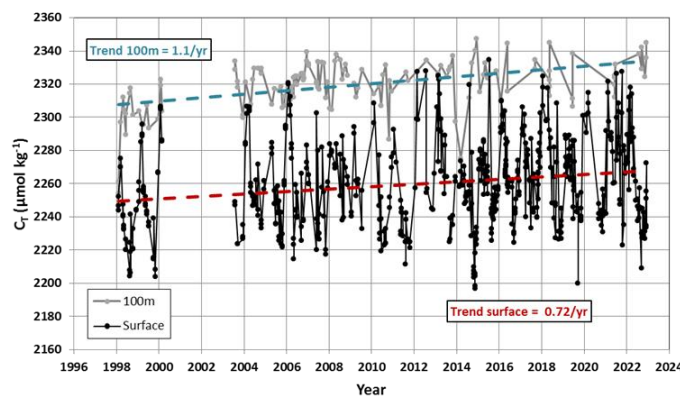
Compared to the open ocean,  $A_T$  concentrations are much higher in the Mediterranean Sea (Copin-Montégut, 1993; Schneider et al., 2007; Álvarez et al., 2023) with values up to  $2600 \mu\text{mol kg}^{-1}$ . The  $A_T$  and  $C_T$  data obtained in 2014-2023 show a clear contrast between the northern and southern regions of the Western Mediterranean Sea with higher concentration in the Ligurian Sea and the Gulf of Lion (Figure 7). This contrast is associated to the circulation and the frontal system in this region (e.g. Barral et al, 2021). New data in the coastal zones in the Gulf of Lion (ACCESS, DICASE, CARBODELTA, COCORICO2, MESURHOBENT) also have very high  $A_T$  and  $C_T$  concentrations ( $A_T > 2600 \mu\text{mol kg}^{-1}$ ;  $C_T > 2350 \mu\text{mol kg}^{-1}$ ). Very low  $A_T$  and  $C_T$  concentrations ( $A_T < 2500 \mu\text{mol kg}^{-1}$ ;  $C_T < 2200 \mu\text{mol kg}^{-1}$ ) were also occasionally observed in the coastal zones (COCORICO2 stations, Petton et al, 2024).

In summer 2022 the Mediterranean Sea experienced an exceptional warming (Figure S6) superposed to the long-term warming in the ocean (Cheng et al, 2024). Such event would impact the internal ocean processes such as thermodynamic, stratification and biological processes (Coppola et al., 2023) and the inter-annual variability and trends of  $C_T$ , pH,  $f\text{CO}_2$  and air-sea  $\text{CO}_2$  fluxes (Yao et al., 2016; Wimart-Rousseau et al., 2023; Chau et al., 2024b). As in 2003, the warming in summer 2022 was associated to the drought event that occurred in Europe and over the Mediterranean Sea (Faranda et al., 2023). In July 2022, the maximum temperature of  $28.42^\circ\text{C}$  was observed at station SOMLIT-Point-B. In the Ligurian Sea the temperature trend was faster in recent years,  $+0.173 \pm 0.072 \text{ }^\circ\text{C}$  per decade over 1990-2010 and  $+0.678 \pm 0.143$  per decade over 2010-2023 (Figure S6). With the new data added in the SNAPO-CO2-v2 synthesis (DYFAMED, MOOSE-ANTARES, and MOOSE-GE) we evaluated a temperature trend of  $+0.84 \pm 0.20 \text{ }^\circ\text{C}$  per decade over 1998-2022 indicating that the discrete sampling captured the property changes at regional scale. Based on the data in the Ligurian Sea the trends of  $C_T$  appeared faster in summer ( $+1.53 \pm 0.46 \mu\text{mol kg}^{-1} \text{ yr}^{-1}$ ) than in winter ( $+0.94 \pm 0.64 \mu\text{mol kg}^{-1} \text{ yr}^{-1}$ , Table 7). On the other hand, the trends of  $A_T$  were the same ( $+0.72 \pm 0.36 \mu\text{mol kg}^{-1} \text{ yr}^{-1}$  in winter and  $+0.69 \pm 0.42 \mu\text{mol kg}^{-1} \text{ yr}^{-1}$  in summer). The trend of  $C_T$  in surface in winter was close to the one derived at 100m (below the Chl-a maximum),  $C_T^{100\text{m}} = +1.10 \pm 0.17 \mu\text{mol kg}^{-1} \text{ yr}^{-1}$  (Figure 8) whereas for  $A_T$  the trend was the same in surface and at depth ( $+0.76 \pm 0.12 \mu\text{mol kg}^{-1} \text{ yr}^{-1}$ ). This suggests that the winter  $C_T$  data recorded the anthropogenic  $\text{CO}_2$  uptake of around  $+1 \mu\text{mol kg}^{-1} \text{ yr}^{-1}$ , Figure S7). Note that, given the observed  $C_T$  trends, the spatial view presented in Figure 7b for 2014-2023 would be the same based on  $C_T$  concentrations normalized to a reference year (not shown). As noted by Touratier and Goyet (2009) the  $C_T$  concentrations in the

605 Mediterranean Sea should increase in parallel with the level of atmospheric anthropogenic CO<sub>2</sub>. For an  
 606 atmospheric CO<sub>2</sub> rate of +2.16 ppm yr<sup>-1</sup> over 1998-2023 (Lan et al., 2024) and at fixed sea surface temperature  
 607 (17.75°C), salinity (38.25) and A<sub>T</sub> (2567 μmol kg<sup>-1</sup>), the theoretical C<sub>T</sub> increase would be +1.24 μmol kg<sup>-1</sup> yr<sup>-1</sup>.  
 608 Interestingly, an anthropogenic flux of -0.3 ±0.02 molC m<sup>-2</sup> yr<sup>-1</sup> in the Mediterranean Sea (Bourgeois et al.,  
 609 2016) would correspond to an increase of C<sub>T</sub> of 1.07 ±0.07 μmol kg<sup>-1</sup> yr<sup>-1</sup> in the top 100 meters. This is again  
 610 close to what is observed in winter or at 100m (Table 7, Figure 8). On the other hand the faster C<sub>T</sub> trend  
 611 observed in surface waters during summer might be associated with a decrease in biological production and/or  
 612 changes in circulation/mixing over time that deserve specific investigations such as analyzed for the oxygen  
 613 budget in this region (Ulses et al, 2021). It is worth noting that the C<sub>T</sub> and A<sub>T</sub> trends in coastal zones of the  
 614 Mediterranean Sea are opposite to those observed offshore: for example at station SOLEMIO (Bay of Marseille,  
 615 Wimart-Rousseau et al., 2020) the C<sub>T</sub> and A<sub>T</sub> concentrations decreased over 2016-2022 and thus opposed to the  
 616 anthropogenic CO<sub>2</sub> signal, indicating that processes such as riverine inputs, advection or biology control the  
 617 carbonate system decadal variability at local scale. This calls for developing dedicated complex biogeochemical  
 618 models to resolve these processes (Barré et al., 2023, 2024), especially when extreme events occurred, such as  
 619 the very hot summer in 2024 with SST up to 30°C in the Mediterranean Sea (Platforms Buoy/Mooring AZUR,  
 620 EOL and La Revellata, data available at <https://dataselection.coriolis.eu.org/>). The data obtained in the  
 621 Mediterranean Sea are important not only to validate biogeochemical models but also to reconstruct the  
 622 carbonate system from A<sub>T</sub> and pCO<sub>2</sub> data (Chau et al., 2024a) as the global A<sub>T</sub>/SSS relationships (e.g. Carter et  
 623 al., 2018) are not suitable for this region.



635 **Figure 7:** Distribution of A<sub>T</sub> (a) and C<sub>T</sub> (b) in μmol kg<sup>-1</sup> in surface waters of the Mediterranean Sea (0-10m) from  
 636 observations over 2014-2023. Figures produced with ODV (Schlitzer, 2018).



651  
652  
653  
654  
655

Figure 8: Time-series of  $C_T$  concentrations in surface (black symbols) and at 100m (grey symbols) in the Ligurian Sea. The trends over 1998-2022 is surface (red) and at 100m (blue) are indicated by dashed lines.

## 656 5.2 The North Atlantic

657

658 The North Atlantic Ocean is an important  $\text{CO}_2$  sink (Takahashi et al. 2009) due to biological activity  
659 during summer, heat loss and deep convection during winter. As a result this region contains high concentrations  
660 of anthropogenic  $\text{CO}_2$  ( $C_{\text{ant}}$ ) in the water column (Khatiwala et al., 2013). Decadal variations of the  $C_{\text{ant}}$   
661 inventories were recently identified at basin scale probably linked to the change of the overturning circulation  
662 (Gruber et al., 2019; Müller et al., 2023; Pérez et al., 2024). This region experienced climate modes such as the  
663 North Atlantic Oscillation (NAO) and the Atlantic Multidecadal Variability (AMV) that imprint variability in  
664 air-sea  $\text{CO}_2$  fluxes at inter-annual to multidecadal scales (e.g. Thomas et al., 2008; Jing et al., 2019;  
665 Landschützer et al., 2019) but not always clearly revealed at regional scale (Metzl et al., 2010; Schuster et al.,  
666 2013; Pérez et al., 2024). In addition it has been recently shown that extreme events such as the marine heat  
667 wave in summer 2023 led to a reduce  $\text{CO}_2$  uptake in this region (Chau et al., 2024b). Although the annual  
668  $\text{CO}_2$  fluxes deduced from Global Ocean Biogeochemical Models (GOBM) seem coherent with the data-products  
669 at basin scale (resp.  $-0.30 \pm 0.07$  and  $-0.24 \pm 0.03$  PgC/yr for the North Atlantic subpolar seasonally stratified,  
670 NA-SPSS biome) the  $p\text{CO}_2$  cycle seasonality is not well simulated (Pérez et al., 2024). Therefore to correct the  
671 GOBMs outputs, comparisons with the observed  $C_T$  and  $A_T$  cycles are also needed.

672 In this context regular sampling in the North Atlantic (OVIDE cruises, Mercier et al., 2015, 2024;  
673 SURATLANT transects, Reverdin et al., 2018) and time-series stations in the Irminger and Iceland Seas  
674 (Ólafsson, et al., 2010; Lange et al., 2024; Yoder et al., 2024) are important to explore the variability of the  
675 biogeochemical properties from seasonal (Figure S8) to decadal scales (Figure 9). The SURATLANT data added  
676 in the SNAPO-CO2-v2 dataset over 2017-2023 offer new observations in the North Atlantic Subpolar Gyre  
677 (NASPG in the NA-SPSS biome) and new transects from Norway to Iceland and reaching the coast of Greenland  
678 (Figure 9). In 2010 the winter NAO was negative, moved to a positive state in 2012-2020 and was again very  
679 low in 2021. The new SURATLANT data after 2017 confirm the cooling and the freshening in the NASPG since  
680 2009 (Holliday et al., 2020; Leseurre et al., 2020; Siddiqui et al., 2024) whereas the most recent data in 2022 and  
681 2023 suggest a reverse trend (increase of salinity and temperature, not shown). After 2016, large  $C_T$  anomalies in  
682 the NASPG were observed. For examples, in April 2019 and 2022, the  $C_T$  concentrations were low compared to  
683 2016 (Figure 9) and opposed to the expected anthropogenic  $\text{CO}_2$  uptake. In September 2023 the  $C_T$   
684 concentrations were much lower than in 2022 (Figure 9) probably linked to biological productivity when the  
685 NAO index was negative (Fröb et al., 2019) as observed in summer 2023 (NAO < -2 in July 2023). Despite these  
686 variability the  $C_T$  trends are relatively well evaluated (Table 7). As in the Mediterranean Sea the  $C_T$  trends in the  
687 NASPG appeared different depending on the season (Figure 9). The  $C_T$  increase was faster in September than in  
688 April (resp.  $+1.09 \pm 0.37 \mu\text{mol kg}^{-1} \text{yr}^{-1}$  and  $+0.78 \pm 0.23 \mu\text{mol kg}^{-1} \text{yr}^{-1}$ ). This is either close to or lower than the  
689 theoretical  $C_T$  increase due to the rising of atmospheric  $\text{CO}_2$  ( $+0.91 \mu\text{mol kg}^{-1} \text{yr}^{-1}$ ) and in the range of recent  
690 results evaluated for the Sub-polar Mode Waters in the Irminger Sea ( $C_{\text{ant}}$  trend =  $0.95 \pm 0.17 \mu\text{mol kg}^{-1} \text{yr}^{-1}$  for  
691 the period 2009-2019, Curbelo-Hernández et al., 2024).



692  
693  
694  
695  
696  
697  
698  
699  
700  
701  
702  
703  
704  
705  
706

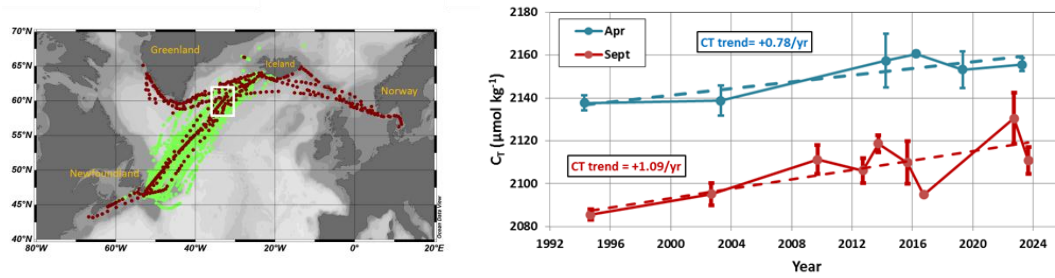


**Figure 9:** Left: Data in SNAPO-CO2-v1 (green) and new data in v2 (brown) from the SURATLANT cruises in 1993-2023 in the North Atlantic. Figure produced with ODV (Schlitzer, 2018). The white box identified the region of selected data around 60°N for the trend analysis. Right: Time-series of average  $C_T$  concentrations in April (blue) and September (red) in this region. The trends for each season are indicated (see also Table 7).

707 **5.3 The Tropical Atlantic**

708  
709  
710  
711  
712  
713  
714  
715  
716  
717  
718  
719  
720

In the Tropical Atlantic, previous studies highlighted the large variability of biogeochemistry and the difficulty in detecting long-term trends of  $C_T$  (e.g. Lefèvre et al., 2021). This is related to the variability of circulation, equatorial upwelling, biological processes (some linked to Saharan dust) and inputs from large rivers (Congo, Amazon and Orinoco). The new data added in version SNAPO-CO2-v2 (Figure S9) show the contrasting zonal  $C_T$  distribution in this region with lower concentrations in low salinity regions of the North Equatorial Counter Current and Guinea Current (Figure 5; Oudot et al., 1995; Takahashi et al., 2014; Broullón et al., 2020; Bonou et al., 2022). For exploring the temporal changes we selected the data in the western region available for at least 10 years and separated the northern and southern sectors. In both regions the  $C_T$  trend is close to  $+3 \mu\text{mol kg}^{-1} \text{ yr}^{-1}$  (Table 7, Figure S9) much higher than the expected anthropogenic signal. In this region where coastal water masses mixes with oceanic waters, the inter-annual variability of  $C_T$  is large and the changes driven by competitive processes (circulation, biological processes). More observations and dedicated models are needed to separate the anthropogenic and natural variability in this region (Pérez et al., 2024).

721  
722 **5.4 The Southern Ocean**

723  
724  
725  
726  
727  
728  
729  
730  
731  
732  
733  
734  
735

In the Southern Ocean there are a few regular multi-annual observations of the carbonate system. Time series of more than 10 years were obtained in the Drake Passage (Munro et al., 2015) and in the Southern Indian Ocean (Leseurre et al., 2022; Metzl et al., 2024b). Observations were also obtained for more than 20 years southeast of New Zealand at the Munida Time Series (MTS) in the subtropical and sub-Antarctic frontal zones (Currie et al., 2011; Vance et al., 2024). To complement these datasets we have added the data collected in the South-Eastern Indian Ocean between Tasmania and Antarctica in the frame of the MINERVE cruises (Figure 10; Brandon et al., 2022). These cruises were conducted from October to March offering each year a view of the seasonal changes between late winter and summer from the sub-Antarctic zone to the coastal zone near Antarctica (Adélie land). In all sectors (here from 45°S to 67°S) the  $C_T$  concentrations were higher in October when the mixed-layer depth (MLD) was deep and were lower during the productive summer season (e.g. Laika et al., 2009; Shadwick et al., 2015). An example is presented at 60°S/151°E from the data obtained along a reoccupied track in 2011-2012 (Figure S10). At this location south of the Polar Front in the POOZ/HNLC area



736 (Permanent Open Ocean Zone/ High Nutrient Low Chlorophyll), the  $C_T$  concentrations were  $+25 \mu\text{mol kg}^{-1}$   
 737 higher in October compared to February. The same seasonal amplitude was observed in the western Indian sector  
 738 of the POOZ (Metzl et al., 2006, 2024b) suggesting that the  $C_T$  seasonality is relatively homogeneous in this  
 739 region corresponding to the Indian SO-SPSS biome (Fay and McKinley, 2014). The difference in the  
 740 climatological  $C_T$  between October and January is on average  $+28.3 \pm 9.8 \mu\text{mol kg}^{-1}$  in the Indian Ocean POOZ  
 741 (Takahashi et al., 2014). Given this seasonality and potential change in the seasonal amplitude over time  
 742 (Gallego et al., 2018; Landschützer et al., 2018; Shadwick et al., 2023) the property trends have to be evaluated  
 743 for October and January-February separately, here over 2002-2012 in the POOZ (Figure 10, Table 7). In both  
 744 seasons, the average  $C_T$  concentrations reached a minimum in 2008 and increased faster in 2008-2012 (up to  
 745  $+4.8 \mu\text{mol kg}^{-1} \text{yr}^{-1}$ ). Interestingly, such acceleration of the trend after 2009 was observed for  $p\text{CO}_2$  at the MTS  
 746 station (Vance et al., 2024). We note that the  $C_T$  trend over 2002-2012 was slightly faster in October (Figure 10)  
 747 probably linked to deeper MLD as suggested from the cooling and the salinity increase observed during this  
 748 season (not shown).

749

750

751

752

753

754

755

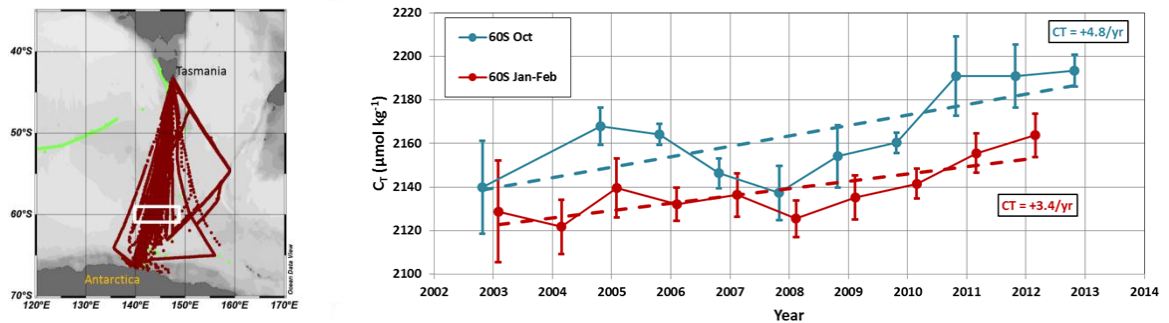
756

757

758

759

760



761 **Figure 10:** Left: Data in SNAPO-CO2-v1 dataset (green) and new data in version v2 (brown) in the South  
 762 eastern Indian Ocean. Figure produced with ODV (Schlitzer, 2018). The white box identified the region of  
 763 selected data around 60°S for the trend analysis. Right: Time-series of average  $C_T$  concentrations in January-  
 764 February (red) and October (blue) around 60°S (white box in the map). The trends for each season are indicated  
 765 (see also Table 7).

766

767

768

769

770

771

772

773

774

In the western Indian sector, the new data in the SNAPO-CO2-v2 dataset from the OISO cruises at high  
 latitudes also recorded a rapid  $C_T$  trend over 5-8 years periods (e.g.,  $+3.4 \mu\text{mol kg}^{-1} \text{yr}^{-1}$  in 2015-2020 at 56°S,  
 Figure 11, Table 7). Although the inter-annual variability of  $C_T$ , between 10 and 20  $\mu\text{mol kg}^{-1}$ , is often  
 recognized (Figure 11), the evaluation of the trends over more than 20 years indicated faster trend in the  
 subtropical Indian Ocean ( $+1.1 \mu\text{mol kg}^{-1} \text{yr}^{-1}$ ) compared to higher latitudes (Indian POOZ,  $+0.6 \mu\text{mol kg}^{-1} \text{yr}^{-1}$ );  
 they are close to the expected anthropogenic signal in these regions ( $+1.1 \mu\text{mol kg}^{-1} \text{yr}^{-1}$  in the subtropics and  
 $+0.8 \mu\text{mol kg}^{-1} \text{yr}^{-1}$  at higher latitudes).

775  
776  
777  
778  
779  
780  
781  
782  
783  
784  
785  
786  
787  
788  
789  
790  
791  
792  
793  
794  
795  
796  
797  
798  
799  
800  
801  
802  
803  
804  
805  
806  
807  
808  
809  
810  
811  
812  
813  
814  
815  
816  
817  
818  
819  
820  
821  
822  
823

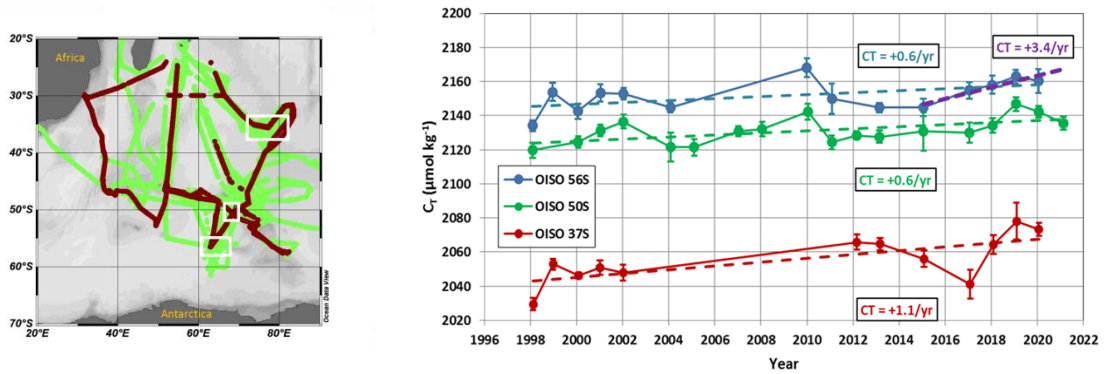


**Figure 11:** Left: Data in SNAPO-CO2-v1 dataset (green) and new data in version v2 (brown) in the South Western Indian Ocean (OISO cruises). Figure produced with ODV (Schlitzer, 2018). The white boxes identified the regions of data selected around 37°S, 50°S and 56°S for the trend analysis. Right: Time-series of average  $C_T$  concentrations in January-February at 37°S (red), 50°S (green) and 56°S (blue). The trends for each region are indicated (see also Table 7).

**Table 7:** Trend of  $C_T$  ( $\mu\text{mol kg}^{-1} \text{yr}^{-1}$ ) and corresponding standard error in selected regions where data are available for more than 10 years. The projects/cruises for selection of the data in each domain are indicated.

Region	Period/Season	$C_T$ trend ( $\mu\text{mol kg}^{-1} \text{yr}^{-1}$ )	Projects/Cruises
North Atlantic (NASPG)	1994-2023 April	+0.78 (0.23)	SURATLANT
North Atlantic (NASPG)	1994-2023 September	+1.09 (0.37)	SURATLANT
West. Trop. Atl. 5N-Eq	2009-2021 April-October	+3.31 (2.13)	AMAZOMIX, PIRATA-BR, TARA
West. Trop. Atl. Eq-10S	2005-2015, April-October	+3.05 (1.64)	CAMFIN-WAT, PIRATA-BR, VOS
Ligurian Sea 8E	1998-2022 Jan-Feb.	+0.94 (0.64)	ANTARES, DYFAMED, MOOSE-GE
Ligurian Sea 8E	1998-2023 July-August	+1.53 (0.46)	ANTARES, DYFAMED, MOOSE-GE
Subtropical Indian 37S	1998-2020 Jan-Feb.	+1.12 (0.36)	OISO
South West. Indian 50S	1998-2021 Jan-Feb.	+0.61 (0.21)	OISO
South West. Indian 56S	1998-2020 Jan-Feb.	+0.58 (0.27)	OISO
South West. Indian 56S	2015-2020 Jan-Feb.	+3.41 (0.73)	OISO
South East. Indian 60S	2002-2012 Jan-Feb.	+3.37 (0.94)	MINERVE, OISO
South East. Indian 60S	2002-2012 October	+4.79 (1.62)	MINERVE

## 824 5.5 The Coastal Zones

825

826 Coastal waters experience enhanced ocean acidification due to increasing  $\text{CO}_2$  uptake, accumulation of  
827 anthropogenic  $\text{CO}_2$  (Bourgeois et al 2016; Laruelle et al, 2018; Roobaert et al, 2024a; Li et al, 2024) and from  
828 local anthropogenic inputs through rivers or from air pollution (e.g. Sarma et al, 2015; Sridvi and Sarma, 2021;  
829 Wimart-Rousseau et al, 2020). The changes of the  $\text{CO}_2$  uptake in coastal zones are also linked to biological  
830 processes (Mathis et al, 2024) or to circulation and local upwelling (Roobaert et al, 2024b), all controlling large  
831 variability of  $A_T$  and  $C_T$  in space and time leading to uncertainties for detecting long-term changes of  $p\text{CO}_2$  and  
832 air-sea  $\text{CO}_2$  fluxes in heterogeneous coastal waters (Dai et al 2022; Resplandy et al, 2024). At seasonal scale,  
833 large differences between observations and models were also identified leading to differences in the coastal

834 ocean CO<sub>2</sub> sink up to 60% (Resplandy et al, 2024). It is thus important to document the seasonal cycles of A<sub>T</sub> and  
835 C<sub>T</sub> to compare and correct models and thus to better predict future changes of biogeochemical properties in  
836 coastal waters and their impact on marine ecosystems. A better understanding of the processes and their  
837 retroaction in the coastal regions is also required regarding Marine Carbon Dioxide Removal (MCDR)  
838 experiments and for their evaluation (e.g. Ho et al, 2023).

839 In the SNAPO-CO<sub>2</sub>-v2 dataset new data have been added in the coastal zones at stations SOMLIT-  
840 Brest, SOMLIT-Roscoff and SOMLIT-Point-B. They extend the period to 2022 or 2023 for temporal analysis.  
841 New data in the French coastal zones have been also included from the COCORICO2 project documented in  
842 detail by Petton et al (2024). The observations in coastal zones could be identified in the MARCATS regions  
843 (Margins and CATchment Segmentation, Laruelle et al, 2013) (Figure 12) where little information is available  
844 for quantifying the ocean CO<sub>2</sub> sink at the decadal scale and for evaluation of the anthropogenic CO<sub>2</sub> uptake  
845 (Regnier et al, 2013; Dai et al, 2022; Li et al, 2024). To explore the change of the observed properties in the  
846 coastal zones and have a flavor of the long-term C<sub>T</sub> trends we selected the time series with at least 10 years of  
847 data (Table 8, Figure 13). Except at high latitudes (Greenland and Antarctic coastal zones), we observed a  
848 warming in coastal zones (not shown). Changes in salinity are also identified (increase or decrease) and results  
849 of the trends are presented for salinity-normalized C<sub>T</sub> at 34, 35 or 38 depending on the region. Although the  
850 inter-annual variability is large in coastal waters, sometimes linked to extreme events (e.g. river discharges), we  
851 observed an increase in N-C<sub>T</sub> at most of the 8 selected locations. The exceptions are the coastal zones in the Gulf  
852 of Lion near the Rhone River and near Tasmania in October.

853 In the Gulf of Lion, the new data in the coastal zone confirmed the first view at the SOLEMIO station  
854 over 2016-2018 (Bay of Marseille, Wimart-Rousseau et al, 2020). In this region the lowest C<sub>T</sub> was observed in  
855 summer 2022 (average C<sub>T</sub> of 2238.6 ±21.0 μmol kg<sup>-1</sup>), much lower than in 2015 (2290.8 ±44.7 μmol kg<sup>-1</sup>). Over  
856 the continental shelf south of Tasmania (MARCATS #34), the trend in N-C<sub>T</sub> was positive in summer but not  
857 significant in October. In October this was associated with an increase in Salinity and in A<sub>T</sub> probably linked to  
858 advective processes via the reversal and variability of the Zeehan or the East Australian currents. From our data a  
859 warming of +0.06°C yr<sup>-1</sup> was identified for both seasons over 2002-2012 as previously observed south of  
860 Tasmania over 1991-2003 impacting the pCO<sub>2</sub> trend and air-sea CO<sub>2</sub> fluxes in this region (Borges et al, 2008).  
861 The difference in the N-C<sub>T</sub> trends in austral summer and spring calls for new detailed studies with extended data  
862 in this region. At high latitude in the Adélie Land (Antarctic coast MARCATS #45), the variability of N-C<sub>T</sub> was  
863 large (range from 2150 to 2200 μmol kg<sup>-1</sup>, Figure 13) and the trend over 10 years in summer was not significant  
864 (Table 8). As opposed to the open zone at 60°S (Figure 10) the C<sub>T</sub> concentrations in the coastal zone near  
865 Antarctica were not increasing, probably linked to competitive processes between anthropogenic uptake, changes  
866 in primary production, mixing or ice melting (Shadwick et al, 2013, 2014). More data are needed to better  
867 evaluate the changes of the carbonate system in Antarctic coastal zones where bottom waters are formed and  
868 transport anthropogenic CO<sub>2</sub> at lower latitudes (Zhang et al, 2023).

869 For the coastal time series SOMLIT where annual trends could be estimated (sampling at monthly  
870 resolution), the N-C<sub>T</sub> increase (+2.1 to 3.4 μmol kg<sup>-1</sup> yr<sup>-1</sup>) is close or higher than the anthropogenic signal leading  
871 to a decrease in pH ranging between -0.05 to -0.06 TS decade<sup>-1</sup>. The new data added in the SNAPO-CO<sub>2</sub>-v2  
872 dataset (2016-2023) confirm the progressive increase in C<sub>T</sub> and the acidification in the western Mediterranean  
873 Sea and in the North-East Atlantic coastal zones (Kapsenberg et al, 2017; Gac et al, 2021).

874  
875  
876  
877  
878  
879  
880  
881  
882  
883  
884  
885  
886  
887  
888  
889  
890  
891  
892  
893  
894  
895  
896  
897  
898  
899  
900  
901  
902  
903  
904  
905  
906  
907  
908  
909  
910  
911  
912  
913  
914  
915  
916  
917  
918  
919  
920  
921  
922  
923  
924  
925  
926  
927  
928  
929  
930  
931  
932  
933

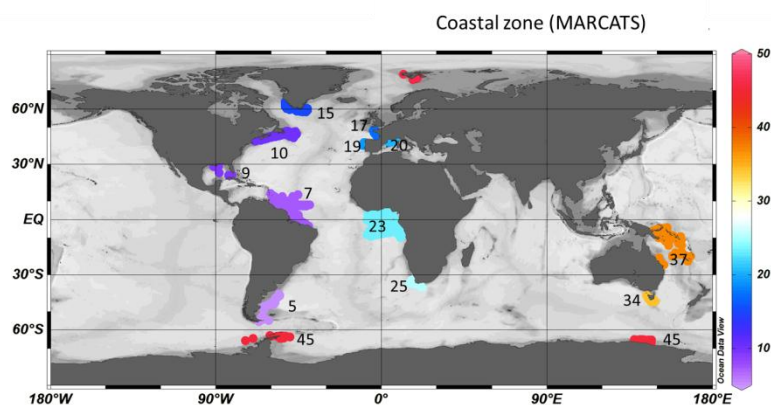


**Figure 12:** Location of  $A_T$  and  $C_T$  data available in the coastal zones in the SNAPO-CO2-v2 dataset. Numbers and Color code identify MARCATS region (Laruelle et al, 2013). Figure produced with ODV (Schlitzer, 2018).

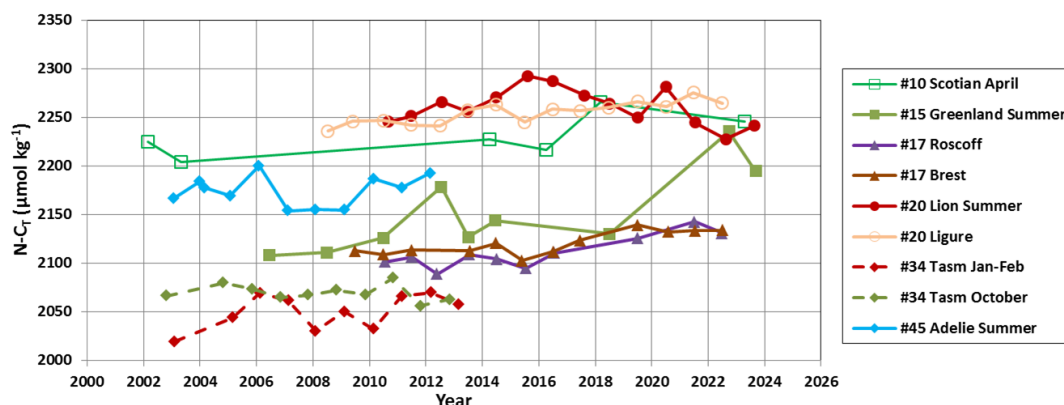


**Figure 13:** Time-series of average  $N-C_T$  concentrations ( $\mu\text{mol kg}^{-1}$ ) in selected MARCATS regions for different period when data are available for ten years or more. The trends and periods for each region are indicated in Table 8.

**Table 8:** Trends of  $N-C_T$  ( $\mu\text{mol kg}^{-1} \text{ yr}^{-1}$ ) and corresponding standard errors in selected coastal regions where data are available for 10 years or more. The projects/cruises for selection of the data in each domain are indicated. MARCATS # regions also identified. Salinity values used for  $C_T$  normalization are indicated.

Region #MARCATS	Period	Season	$N-C_T$ Trend ( $\mu\text{mol kg}^{-1} \text{ yr}^{-1}$ )	Salinity	Projects/Cruises
Scotian #10	2002-2023	March-April	+1.71 (0.97)	35	SURATLANT
Greenland #15	2006-2023	June-mid-Sept	+5.77 (1.62)	35	OVIDE, SURATLANT
Roscoff #17	2010-2022	All season	+3.40 (0.76)	35	CHANNEL, COCORICO2, SOMLIT ROSCOFF
Bay of Brest #17	2009-2022	All seasons	+2.17 (0.52)	35	SOMLIT-Brest, COCORICO2, ECOSCOPIA,
LION#20	2010-2023	June-Sept	-1.19 (1.25)	38	COCORICO2, MOOSE-GE, SOLEMIO (a)
LIGURE#20	2008-2022	All seasons	+2.12 (0.36)	38	SOMLIT-Point-B, MOOSE-GE
Tasmania #34	2003-2013	Jan-Feb	+2.73 (1.72)	35	MINERVE, OISO
Tasmania #34	2002-2012	Oct	-0.65 (0.89)	35	MINERVE, OISO
Adélie #45	2002-2012	Dec-Feb	+0.63 (0.70)	34	MINERVE, OISO

(a) For LION, some data in summer were also used from punctual cruises: AMOR-BFlux, CARBORHONE, DICASE, LATEX, MESURHOBENT, MISSRHODIA2 and MOLA.

## 934 6 Summary and suggestions

935

936 This work extends in time and in new oceanic regions the  $A_T$  and  $C_T$  data presented in the first SNAPO-  
937 CO<sub>2</sub> synthesis (Metzl et al, 2024a). It includes now more than 67 000 surface and water column observations in  
938 all oceanic basins, in the Mediterranean Sea, in the coastal zones, near coral reefs, and in rivers. The data  
939 synthesized in version v2 are based on measurements of  $A_T$  and  $C_T$  performed between 1993 and 2023 with an  
940 accuracy of  $\pm 4 \mu\text{mol kg}^{-1}$ . Based on a secondary quality control, 91% of the  $A_T$  and  $C_T$  data are considered as  
941 good (WOCE Flag 2) and 6% probably good (Flag 3). For the open ocean this synthesis complements the  
942 SOCAT, GLODAP and SPOTS data products (Bakker et al., 2016; Lauvset et al., 2024; Lange et al, 2024). For  
943 the coastal sites this also complements the synthesis of coastal time-series in the Iberian Peninsula (Padin et al,  
944 2020), in the Canadian Atlantic continental shelf (Gibb et al, 2023) and around North America (Fassbender et al.,  
945 2018; Jiang et al., 2021; Jiang et al 2024, in prep). The SNAPO-CO<sub>2</sub> dataset enables to investigate the seasonal  
946 cycles, the inter-annual variability and the decadal trends of  $A_T$  and  $C_T$  in various oceanic provinces. The same  
947 temporal analyses could be investigated for other carbonate system properties such as  $f\text{CO}_2$  or pH calculated  
948 from  $A_T$  and  $C_T$  for air-sea CO<sub>2</sub> flux estimates or ocean acidification studies (Figure 14).

949

950

951

952

953

954

955

956

957

958

959

960

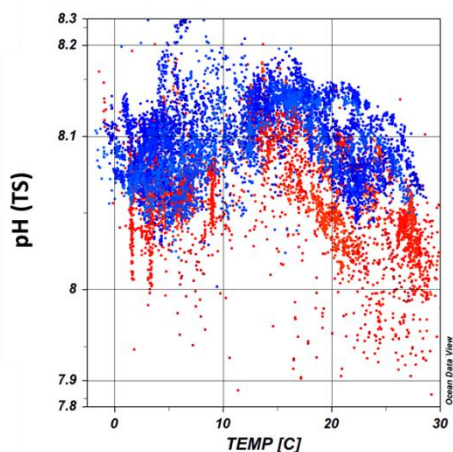
961

962

963

964

965



966 **Figure 14:** An example of observed ocean acidification derived from the SNAPO-CO<sub>2</sub>-v2 dataset: pH (TS)  
967 calculated with  $A_T$  and  $C_T$  data are presented as a function of temperature (°C) for years 1998-2002 (blue  
968 symbols) and 2020-2023 (red symbols) and for salinity > 33 (Nb data selected with flag 2 = 11994). In recent  
969 years the pH was lower. Figure produced with ODV (Schlitzer, 2018).  
970

971 In almost all regions the new data in 2021-2023 indicated that the  $C_T$  concentrations were higher in  
972 recent years. In regions where data are available for more than 2 decades, the time-series show an increase of sea  
973 surface  $C_T$  (North Atlantic, Southern Indian Ocean and Ligurian Sea) with a rate close to or higher than the  
974 changes expected from anthropogenic CO<sub>2</sub> uptake. It is also recognized that at seasonal scale the  $C_T$  trends could  
975 be different. However, with the data in hand, the long-term trend of  $C_T$  cannot be quantified with confidence to  
976 compare with the anthropogenic carbon uptake in some regions. This is the case in the eastern tropical Atlantic  
977 subject to high inter-annual variability (Lefèvre et al., 2021, 2024) although new data have been added over  
978 2005-2022 in this region (Table 1, Figure S9). When data are available for less than a decade the increase in  $C_T$   
979 was observed but the trend was uncertain due to large inter-annual variability (e.g. Adélie Land). An exception  
980 was identified in the coastal zone in the Gulf of Lion (Mediterranean Sea) where summer data since 2010 present

981 a decrease in  $C_T$  most pronounced since 2015 ( $C_T$  trend =  $-5.2 \pm 1.5 \mu\text{mol kg}^{-1} \text{yr}^{-1}$ ). Such  $C_T$  decrease over 10  
982 years was also observed at the Hawaii Ocean Time series, HOT over 2010-2020 (Dore et al, 2009,  
983 <https://hahana.soest.hawaii.edu/hot/hotco2/hotco2.html>, last access: 27 August 2024).

984 Although the  $A_T$  concentrations present significant inter-annual variability such as in the NASPG, in the  
985 Topical Atlantic or the Adélie land and coastal zones,  $A_T$  appears relatively constant over time except at these  
986 locations. In the open ocean, we observed an increase of  $A_T$  in the Southern Ocean south of the Polar Front  
987 around  $60^\circ\text{S}$  in 2003-2012 not directly linked to salinity. In the coastal zones a decrease of  $A_T$  was pronounced  
988 south of Greenland. In the coast in the Gulf of Lion, as observed for  $C_T$ ,  $A_T$  decreased ( $A_T$  trend =  $-2.8 \pm 1.2 \mu\text{mol}$   
989  $\text{kg}^{-1} \text{yr}^{-1}$ ). This is opposed to the changes observed in the Ligurian Sea at station SOMLIT-Point-B, where  $C_T$  and  
990  $A_T$  increased over 2007-2015 (Kapsenberg et al, 2017) highlighting the contrasting  $C_T$  and  $A_T$  trends in the  
991 Mediterranean coastal zones where ocean acidification is detected (here over 2008-2022, pH trend of  $-0.048$   
992  $\pm 0.003 \text{decade}^{-1}$ ). With the continuous warming, reduced stratification and the rapid pH change observed in the  
993 Mediterranean Sea, how the marine ecosystems will respond in the future should be addressed (e.g. Howes et al,  
994 2015; Maugendre et al 2015; Lacoue-Labarthe et al, 2016). The SNAPO-CO2-v2 dataset could also be used to  
995 explore and analyze the changes of the carbonate system occurring during extreme events such as marine heat  
996 waves, rapid freshening, deep convection or high phytoplankton bloom events.

997 This dataset could also serve for validating autonomous platforms capable of measuring pH and  $f\text{CO}_2$   
998 properties (Sarmiento et al, 2023) and, along with other synthesis products (Jiang et al, 2024 in prep.), provides  
999 an additional reference dataset for the development and validation of regional biogeochemical models for  
1000 simulating air-sea  $\text{CO}_2$  fluxes. Thanks to the RECCAP2 stories, it has been recognized that Ocean  
1001 Biogeochemical Models present biases in the seasonal cycle of  $C_T$  and  $A_T$  due to inadequate representation of  
1002 biogeochemical cycles (e.g. Hauck et al, 2023; Rodgers et al, 2023; Sarma et al, 2023; Pérez et al, 2024;  
1003 Resplandy et al, 2024). The SNAPO-CO2-v2 dataset could be used to guide analyses for regional or global  
1004 biogeochemical models for  $A_T$  and  $C_T$  comparison and validation from seasonal to decadal scales. Our dataset is  
1005 also essential for training and validating neural networks capable of predicting variables in the carbonate system  
1006 (e.g. Fourier et al, 2020; Chau et al, 2024a; Gregor et al, 2024), thereby enhancing observations of marine  $\text{CO}_2$  at  
1007 different spatial and temporal scales. Furthermore, we encourage the use of this dataset (or part of it), at sea or  
1008 prior going to sea for cruise planning. Indeed, using the approach of Davis and Goyet (2021) which takes into  
1009 account the multiple constraints (ship-time, number of samples, etc.), it is possible to determine the most  
1010 appropriate sampling strategy (Guglielmi et al., 2022, 2023), to reach the specific scientific objectives of each  
1011 cruise.

1012 The data presented here are available online on the Seano server (<https://doi.org/10.17882/102337>) in a  
1013 file identifying version v1 and v2. The sources of the original datasets (doi) with the associated references are  
1014 listed in the Supplementary Material (Tables S3, S4). As for version v1 we invite the users to comment on any  
1015 anomaly that would have not been detected or to suggest potential misqualification of data in the present product  
1016 (e.g. data probably good although assigned with flag 3, probably wrong). As for SOCAT or GLODAP, we  
1017 expect to update the SNAPO-CO2 dataset once new observations are obtained and controlled.

1018

1019 **7 Data availability**

1020 Data presented in this study are available at Seanoe (Metzl et al, 2024d, <https://www.seanoe.org>,  
1021 <https://doi.org/10.17882/102337>. See also <https://doi.org/10.17882/95414> for version V1. The dataset is also  
1022 available at <https://explore.webodv.awi.de/ocean/carbon/snapo-co2/>

1023

1024 *Author contributions.* NM prepared the data synthesis, the figures and wrote the draft of the manuscript with  
1025 contributions from all authors. JF measured the discrete samples since 2014, with the help from CM and CLM,  
1026 and prepared the individual reports for each project. NM and JF pre-qualified the discrete  $A_T/C_T$  data. CLM and  
1027 NM are co-Is of the ongoing OISO project and qualified the underway  $A_T/C_T$  data from OISO cruises. FT and  
1028 CG were PIs of the MINERVE cruises. All authors have contributed either to organizing cruises, sample  
1029 collection and/or data qualification, and reviewed the manuscript.

1030

1031 *Competing interest.* The authors have the following competing interests: At least one of the (co-)authors is a  
1032 member of the editorial board of Earth System Science Data

1033

1034 *Acknowledgments.* Most of the  $A_T$  and  $C_T$  data presented in this study were measured at the SNAPO-CO2 facility  
1035 (Service National d'Analyse des Paramètres Océaniques du CO2) housed by the LOCEAN laboratory and part of  
1036 the OSU ECCE Terra at Sorbonne University and INSU/CNRS analytical services. Support by INSU/CNRS, by  
1037 OSU ECCE Terra and by LOCEAN, is gratefully acknowledged as well as support by different French "Services  
1038 nationaux d'Observations", such as OISO/CARAUS, SOMLIT, PIRATA, SSS and MOOSE. We thank the  
1039 research infrastructure ICOS (Integrated Carbon Observation System) France for funding a large part of the  
1040 analyses. We thank the IRD (Institut de Recherche pour le Développement) and the French-Brazilian IRD-  
1041 FAPEMA program for funding observations in the tropical Atlantic. We thank the French oceanographic fleet  
1042 ("Flotte océanographique française") for financial and logistic support for most cruises listed in this synthesis  
1043 and for the OISO program (<https://campagnes.flotteoceanographique.fr/series/228/>). We acknowledge the  
1044 MOOSE program (Mediterranean Ocean Observing System for the Environment,  
1045 <https://campagnes.flotteoceanographique.fr/series/235/fr/>) coordinated by CNRS-INSU and the Research  
1046 Infrastructure ILICO (CNRS-IFREMER). The CocoriCO2 project was founded by European Maritime and  
1047 Fisheries Fund (grant no. 344, 2020–2023) and benefited from a subsidy from the Adour-Garonne water agency.  
1048 We thank the following programs coordinated by A. Tribollet which have contributed to the acquisition of the  
1049 data in Mayotte: CARBODISS funded by CNRS-INSU in 2018-2019, Future Maore reefs funded by Next  
1050 Generation UE-France Relance in 2021-2023, and OA-ME funded by a Belmont Forum International (ANR) in  
1051 2020-2026. We thank the program Mermex-Mistrals CNRS for supporting AMOR-BFlux, CARBORHONE,  
1052 DICASE and MESURHOBENT cruises and the program EC2CO-INSU for supporting MISSRHODIA2 cruise.  
1053 The ACCESS project was supported by CNRS MISTRALS and the DELTARHONE-1 by EC2CO-INSU. The  
1054 ACIDHYPO project was founded by CNRS International Emerging Actions; we thank Captain and crew of the  
1055 R/V Savannah from the Skidaway Institute of Oceanography (University of Georgia) for their support and  
1056 technical assistance during the operations at sea. The AMAZOMIX project was funded by French  
1057 Oceanographic Fleet, INSU (LEFE), IRD (LMI TAPICOA), CNES (TOSCA MIAMAZ project) and by the  
1058 French-Brazilian international program GUYAMAZON. The OISO program was supported by the French  
1059 institutes INSU (Institut National des Sciences de l'Univers) and IPEV (Institut Polaire Paul-Emile Victor), OSU



1060 Ecce-Terra (at Sorbonne Université), and the French program SOERE/Great-Gases. We also thank the Research  
1061 Infrastructure ILICO (<https://www.ir-ilico.fr>). We warmly thank Alain Poisson who initiated the MINERVE  
1062 program and performed many of the measurements onboard R/V Astrolabe from 2002 through 2018. We thank  
1063 all colleagues and students who participated to the cruises and have carefully collected the precious seawater  
1064 samples. We thank Frédéric Merceur (IFREMER) for preparing the page and data availability on Seanoë and  
1065 Reiner Schlitzer (AWI) for including the SNAPO-CO<sub>2</sub> dataset in the ODV portal. We thank the associated editor  
1066 Sebastiaan van de Velde to manage this manuscript, and Kim Currie and Toste Tanhua for their suggestions that  
1067 helped to improve this article.

1068

## 1069 **References:**

1070

1071 Ait Ballagh, F.E., Rabouille, C., Andrieux-Loyer, F. et al. Spatial Variability of Organic Matter and Phosphorus  
1072 Cycling in Rhône River Prodelta Sediments (NW Mediterranean Sea, France): a Model-Data Approach.  
1073 *Estuaries and Coasts* 44, 1765–1789, <https://doi.org/10.1007/s12237-020-00889-9>, 2021

1074

1075 Álvarez, M., Catalá, T. S., Civitarese, G., Coppola, L., Hassoun, A. E.R., Ibello, V., Lazzari, P., Lefevre, D.,  
1076 Macías, D., Santinelli, C. and Ulses, C.: Chapter 11 - Mediterranean Sea general biogeochemistry, Editor(s):  
1077 Katrin Schroeder, Jacopo Chiggiato, *Oceanography of the Mediterranean Sea*, Elsevier, Pages 387-451,  
1078 <https://doi.org/10.1016/B978-0-12-823692-5.00004-2>, 2023.

1079

1080 Bakker, D. C. E., Pfeil, B., Landa, C. S., Metzl, N., O'Brien, K. M., Olsen, A., Smith, K., Cosca, C., Harasawa,  
1081 S., Jones, S. D., Nakaoka, S.-I., Nojiri, Y., Schuster, U., Steinhoff, T., Sweeney, C., Takahashi, T., Tilbrook, B.,  
1082 Wada, C., Wanninkhof, R., Alin, S. R., Balestrini, C. F., Barbero, L., Bates, N. R., Bianchi, A. A., Bonou, F.,  
1083 Boutin, J., Bozec, Y., Burger, E. F., Cai, W.-J., Castle, R. D., Chen, L., Chierici, M., Currie, K., Evans, W.,  
1084 Featherstone, C., Feely, R. A., Fransson, A., Goyet, C., Greenwood, N., Gregor, L., Hankin, S., Hardman-  
1085 Mountford, N. J., Harlay, J., Hauck, J., Hoppema, M., Humphreys, M. P., Hunt, C. W., Huss, B., Ibáñez, J. S.  
1086 P., Johannessen, T., Keeling, R., Kitidis, V., Körtzinger, A., Kozyr, A., Krasakopoulou, E., Kuwata, A.,  
1087 Landschützer, P., Lauvset, S. K., Lefèvre, N., Lo Monaco, C., Manke, A., Mathis, J. T., Merlivat, L., Millero, F.  
1088 J., Monteiro, P. M. S., Munro, D. R., Murata, A., Newberger, T., Omar, A. M., Ono, T., Paterson, K., Pearce, D.,  
1089 Pierrot, D., Robbins, L. L., Saito, S., Salisbury, J., Schlitzer, R., Schneider, B., Schweitzer, R., Sieger, R.,  
1090 Skjelvan, I., Sullivan, K. F., Sutherland, S. C., Sutton, A. J., Tadokoro, K., Telszewski, M., Tuma, M., Van  
1091 Heuven, S. M. A. C., Vandemark, D., Ward, B., Watson, A. J., and Xu, S.: A multi-decade record of high-quality  
1092 fCO<sub>2</sub> data in version 3 of the Surface Ocean CO<sub>2</sub> Atlas (SOCAT), *Earth Syst. Sci. Data*, 8, 383-413,  
1093 doi:10.5194/essd-8-383-2016. 2016.

1094

1095 Barral, Q-B., Zakardjian, B. Dumas, F., Garreau, P., Testor, P., and Beuvier, J.: Characterization of fronts in the  
1096 Western Mediterranean with a special focus on the North Balearic Front, *Progress in Oceanography*, Volume  
1097 197, 102636, <https://doi.org/10.1016/j.pocean.2021.102636>. 2021

1098

1099 Barré, L., Diaz, F., Wagener, T., Van Wambeke, F., Mazoyer, C., Yohia, C., and Pinazo, C.: Implementation and  
1100 assessment of a model including mixotrophs and the carbonate cycle (Eco3M\_MIX-CarbOx v1.0) in a highly  
1101 dynamic Mediterranean coastal environment (Bay of Marseille, France) – Part 1: Evolution of ecosystem  
1102 composition under limited light and nutrient conditions, *Geosci. Model Dev.*, 16, 6701–6739,  
1103 <https://doi.org/10.5194/gmd-16-6701-2023>, 2023.

1104

1105 Barré, L., Diaz, F., Wagener, T., Mazoyer, C., Yohia, C., and Pinazo, C.: Implementation and assessment of a  
1106 model including mixotrophs and the carbonate cycle (Eco3M\_MIX-CarbOx v1.0) in a highly dynamic  
1107 Mediterranean coastal environment (Bay of Marseille, France) – Part 2: Towards a better representation of total  
1108 alkalinity when modeling the carbonate system and air–sea CO<sub>2</sub> fluxes, *Geosci. Model Dev.*, 17, 5851–5882,  
1109 <https://doi.org/10.5194/gmd-17-5851-2024>, 2024.

1110

1111 BERTRAND Arnaud, DE SAINT LEGER Emmanuel, KOCH-LARROUY Ariane : AMAZOMIX 2021 cruise,  
1112 RV Antea, <https://doi.org/10.17600/18001364>, 2021



1113  
1114 Bittig, H.C., Steinhoff, T., Claustre, H., Fiedler, B., Williams, N.L., Sauzède, R., Körtzinger, A. and Gattuso, J.-  
1115 P.: An Alternative to Static Climatologies: Robust Estimation of Open Ocean CO<sub>2</sub> Variables and Nutrient  
1116 Concentrations From T, S, and O<sub>2</sub> Data Using Bayesian Neural Networks. *Front. Mar. Sci.* 5:328. doi:  
1117 10.3389/fmars.2018.00328, 2018  
1118  
1119 Bonou, F.K., Noriega, C., Lefèvre, N., Araujo, M.: Distribution of CO<sub>2</sub> parameters in the Western Tropical  
1120 Atlantic Ocean, *Dynamics of Atmospheres and Oceans*, 73: 47-60  
1121 <http://dx.doi.org/10.1016/j.dynatmoce.2015.12.001>, 2016  
1122  
1123 Bonou, F., Medeiros, C., Noriega, C., Araujo, M., Aubains Hounsou-Gbo, A., and Lefèvre N. : A comparative  
1124 study of total alkalinity and total inorganic carbon near tropical Atlantic coastal regions. *J Coast Conserv* 26, 31,  
1125 <https://doi.org/10.1007/s11852-022-00872-5>, 2022  
1126  
1127 Borges A.V., B. Tilbrook, N. Metzl, A. Lenton and B. Delille: Inter-annual variability of the carbon dioxide  
1128 oceanic sink south of Tasmania, *Biogeosciences*, 5, 141-155. <https://doi.org/10.5194/bg-5-141-2008>, 2008  
1129  
1130 Bourgeois, T., J. C. Orr, L. Resplandy, J. Terhaar, C. Ethé, M. Gehlen, and L. Bopp: Coastal-ocean uptake of  
1131 anthropogenic carbon. *Biogeosciences*, 13, 4167-4185, doi: 10.5194/bg-13-4167-2016., 2016  
1132  
1133 BOURLES Bernard (1997) PIRATA, <https://doi.org/10.18142/14>  
1134  
1135 BOURLES Bernard (2019) PIRATA FR29 cruise, RV Thalassa, <https://doi.org/10.17600/18000875>  
1136  
1137 BOURLES Bernard, LLIDO Jérôme (2020) PIRATA FR30 cruise, RV Thalassa,  
1138 <https://doi.org/10.17600/18000690>  
1139  
1140 BOURLES Bernard, LLIDO Jérôme (2022) PIRATA FR32 cruise, RV Thalassa,  
1141 <https://doi.org/10.17600/18001832>  
1142  
1143 Bozec Y., Cariou, T., Mace, E., Morin, P., Thuillier, D., Vernet, M.: Seasonal dynamics of air-sea CO<sub>2</sub> fluxes in  
1144 the inner and outer Loire estuary (NW Europe). *Estuarine Coastal And Shelf Science*, 100, 58-71.  
1145 <https://doi.org/10.1016/j.ecss.2011.05.015>, 2012  
1146  
1147 BOZEC Yann (2009) CO<sub>2</sub>ARVOR 3 cruise, RV Côtes De La Manche, <https://doi.org/10.17600/9480170>  
1148  
1149 BOZEC Yann (2009) CO<sub>2</sub>ARVOR 2 cruise, RV Côtes De La Manche, <https://doi.org/10.17600/9480110>  
1150  
1151 BOZEC Yann (2009) CO<sub>2</sub>ARVOR 1 cruise, RV Thalia, <https://doi.org/10.17600/9070070>  
1152  
1153 Brandon, M., C. Goyet, F. Touratier, N. Lefèvre, E. Kestenare, and R. Morrow : Spatial and temporal variability  
1154 of the physical, carbonate and CO<sub>2</sub> properties in the Southern Ocean surface waters during austral summer  
1155 (2005-2019). *Deep Sea Res. Part I*, 187, 103836, <https://doi.org/10.1016/j.dsr.2022.103836>. 2022  
1156  
1157 Broullón, D., Pérez, F. F., Velo, A., Hoppema, M., Olsen, A., Takahashi, T., Key, R. M., Tanhua, T., González-  
1158 Dávila, M., Jeansson, E., Kozyr, A., and van Heuven, S. M. A. C.: A global monthly climatology of total  
1159 alkalinity: a neural network approach, *Earth Syst. Sci. Data*, 11, 1109–1127, [https://doi.org/10.5194/essd-11-](https://doi.org/10.5194/essd-11-1109-2019)  
1160 1109-2019. 2019  
1161  
1162 Broullón, D., Pérez, F. F., Velo, A., Hoppema, M., Olsen, A., Takahashi, T., Key, R. M., Tanhua, T., Santana-  
1163 Casiano, J. M., and Kozyr, A.: A global monthly climatology of oceanic total dissolved inorganic carbon: a

1164 neural network approach, *Earth Syst. Sci. Data*, 12, 1725–1743, <https://doi.org/10.5194/essd-12-1725-2020>.  
1165 2020  
1166  
1167 CARIOU Thierry, BOZEC Yann (2010) CO2ARVOR 4 cruise, RV Thalia, <https://doi.org/10.17600/10070040>  
1168  
1169 Carter, B. R., Feely, R. A., Williams, N. L., Dickson, A. G., Fong, M. B., and Takeshita, Y.: Updated methods  
1170 for global locally interpolated estimation of alkalinity, pH, and nitrate. *Limnology and Oceanography: Methods*,  
1171 16: 119-131. doi: 10.1002/lom3.10232, 2018  
1172  
1173 Chau, T.-T.-T., Gehlen, M., Metzl, N., and Chevallier, F.: CMEMS-LSCE: a global, 0.25°, monthly  
1174 reconstruction of the surface ocean carbonate system, *Earth Syst. Sci. Data*, 16, 121–160,  
1175 <https://doi.org/10.5194/essd-16-121-2024>, 2024a.  
1176  
1177 Chau, T.-T.-T., Chevallier, F., and Gehlen, M.: Global analysis of surface ocean CO<sub>2</sub> fugacity and air-sea fluxes  
1178 with low latency. *Geophysical Research Letters*, 51, e2023GL106670. <https://doi.org/10.1029/2023GL106670>,  
1179 2024b  
1180  
1181 Cheng, L. J., Abraham, J., Zhu, J., Trenberth, K. E., Fasullo, J., Boyer, T., Locarnini, R., Zhang, B., Yu, F. J.,  
1182 Wan, L. Y., Chen, X. R., Song, X. Z., Liu, Y. L., and Mann, M. E.: Record-setting ocean warmth continued in  
1183 2019, *Adv. Atmos. Sci.*, 37, 137-142. <https://doi.org/10.1007/s00376-020-9283-7>, 2020  
1184  
1185 Cheng, L., Abraham, J., Trenberth, K.E. et al. New Record Ocean Temperatures and Related Climate Indicators  
1186 in 2023. *Adv. Atmos. Sci.*, <https://doi.org/10.1007/s00376-024-3378-5>, 2024  
1187  
1188 Conan, P., Guieux, A., and Vuillemin, R.: MOOSE (MOLA), <https://doi.org/10.18142/234>, 2020.  
1189  
1190 Copin-Montégut, C.: Alkalinity and carbon budgets in the Mediterranean Sea, *Global Biogeochemical Cycles*,  
1191 vol. 7, pp. 915–925, 1993.  
1192  
1193 Coppola, L., and Diamond-Riquier, E.: MOOSE (DYFAMED), <https://doi.org/10.18142/131>, 2008.  
1194  
1195 Coppola Laurent, Diamond Riquier Emilie, Carval Thierry, Irisson Jean-Olivier, Desnos Corinne: Dyfamed  
1196 observatory data. SEANOE. <https://doi.org/10.17882/43749>, 2024  
1197  
1198 Coppola, L., Fourier, M., Pasqueron de Fommervault, O., Poteau, A., Riquier, E. D. and Béquery, L.:  
1199 Highresolution study of the air-sea CO<sub>2</sub> flux and net community oxygen production in the Ligurian Sea by a  
1200 fleet of gliders. *Front. Mar. Sci.* 10:1233845. doi: 10.3389/fmars.2023.1233845, 2023  
1201  
1202 Curbelo-Hernández, D., Pérez, F. F., González-Dávila, M., Gladyshev, S. V., González, A. G., González-  
1203 Santana, D., Velo, A., Sokov, A., and Santana-Casiano, J. M.: Ocean Acidification trends and Carbonate System  
1204 dynamics in the North Atlantic Subpolar Gyre during 2009–2019, *EGUsphere* [preprint],  
1205 <https://doi.org/10.5194/egusphere-2024-1388>, 2024.  
1206  
1207 Currie, K. I., Reid, M. R., and Hunter, K. A.: Interannual variability of carbon dioxide draw-down by  
1208 subantarctic surface water near New Zealand, *Biogeochemistry*, 104, 23–34, [https://doi.org/10.1007/s10533-009-](https://doi.org/10.1007/s10533-009-9355-3)  
1209 9355-3, 2011.  
1210  
1211 Cyronak, T., Santos, I. R., Erler, D. V., and Eyre, B. D.: Groundwater and porewater as major sources of  
1212 alkalinity to a fringing coral reef lagoon (Muri Lagoon, Cook Islands), *Biogeosciences*, 10, 2467–2480,  
1213 <https://doi.org/10.5194/bg-10-2467-2013>, 2013.  
1214  
1215 Dai, M., J. Su, Y. Zhao, E. E. Hofmann, Z. Cao, W. –J. Cai, J. Gan, F. Lacroix, G. G. Laruelle, F. Meng, J. D.  
1216 Müller, P. A.G. Regnier, G. Wang, Z. Wang, 2022. Carbon Fluxes in the Coastal Ocean: Synthesis, *Boundary*

1217 Processes and Future Trends, *Annual Review of Earth and Planetary Sciences*, 50:1, 593-626,  
1218 <https://doi.org/10.1146/annurev-earth-032320-090746>, 2022  
1219  
1220 Davis D. and Goyet, C.: Balanced Error Sampling with applications to ocean biogeochemical sampling.  
1221 Collection études, Presses Universitaires de Perpignan, 224p. ISBN : 978-2-35412-452-6, 2021  
1222  
1223 Dickson, A. G., Sabine, C. L., and Christian, J. R.: Guide to best practices for ocean CO<sub>2</sub> measurements, North  
1224 Pacific Marine Science Organization, Sidney, British Columbia, 191, <https://doi.org/10.25607/OBP-1342>, 2007.  
1225  
1226 DOE: Handbook of Methods for Analysis of the Various Parameters of the Carbon Dioxide System in Seawater;  
1227 version 2, A.G. Dickson et C. Goyet, eds, ORNL/CDIAC-74, <https://doi.org/10.2172/10107773>, 1994.  
1228  
1229 Doney, S. C., Fabry, V. J., Feely, R. A., and Kleypas, J. A., Ocean acidification: The other CO<sub>2</sub> problem. *Annual*  
1230 *Review of Marine Science*, 1(1), 169–192. 10.1146/annurev.marine.010908.163834, 2009  
1231  
1232 Doney, S. C., Busch, D. S., Cooley, S. R., and Kroeker, K. J.: The Impacts of Ocean Acidification on Marine  
1233 Ecosystems and Reliant Human Communities. *Annual Review of Environment and Resources* 45:1,  
1234 <https://doi.org/10.1146/annurev-environ-012320-083019>. 2020  
1235  
1236 Dumoulin J-P, Pozzato L., Rassman J., Toussaint F., Fontugne M., Tisnerat-Laborde N., Beck L., Caffy I.,  
1237 Delque-Kolic E., Moreau C., Rabouille C. : Isotopic Signature (13C, 14C) of DIC in Sediment Pore Waters: An  
1238 Example from the Rhone River Delta. *Radiocarbon*, 60(5), 1465-1481. <https://doi.org/10.1017/RDC.2018.111>,  
1239 2018.  
1240  
1241 Dumoulin J-P, Rabouille C, Pourtout S, Bombled B, Lansard B, Caffy I, Hain S, Perron M, Sieudat M, Thellier  
1242 B, Delqué-Koli E, Moreau C, Beck L (2022). : Identification in Pore Waters of Recycled Sediment Organic  
1243 Matter Using the Dual Isotopic Composition of Carbon (13C and 14C): New Data From the Continental Shelf  
1244 Influenced by the Rhône River. *Radiocarbon*, 64(6), 1617-1627. <https://doi.org/10.1017/RDC.2022.71>, 2022.  
1245  
1246 Edmond, J. M.: High precision determination of titration alkalinity and total carbon dioxide content of sea water  
1247 by potentiometric titration, *Deep-Sea Res.*, 17, 737–750, [https://doi.org/10.1016/0011-7471\(70\)90038-0](https://doi.org/10.1016/0011-7471(70)90038-0), 1970.  
1248  
1249 Eyring, V., Righi, M., Lauer, A., Evaldsson, M., Wenzel, S., Jones, C., Anav, A., Andrews, O., Cionni, I., Davin,  
1250 E. L., Deser, C., Ehbrecht, C., Friedlingstein, P., Gleckler, P., Gottschaldt, K.-D., Hagemann, S., Juckes, M.,  
1251 Kindermann, S., Krasting, J., Kunert, D., Levine, R., Loew, A., Mäkelä, J., Martin, G., Mason, E., Phillips, A. S.,  
1252 Read, S., Rio, C., Roehrig, R., Senfleben, D., Sterl, A., van Ulft, L. H., Walton, J., Wang, S., and Williams, K.  
1253 D.: ESMValTool (v1.0) – a community diagnostic and performance metrics tool for routine evaluation of Earth  
1254 system models in CMIP, *Geosci. Model Dev.*, 9, 1747-1802, doi:10.5194/gmd-9-1747-2016, 2016.  
1255  
1256 Fabry, V. J., Seibel, B. A., Feely, R. A. and Orr, J. C.: Impacts of ocean acidification on marine fauna and  
1257 ecosystem processes. *ICES J. Mar. Sci.* 65, 414–432. <https://doi.org/10.1093/icesjms/fsn048>, 2008.  
1258  
1259 Faranda, D., Pascale, S., Bulut, B.: Persistent anticyclonic conditions and climate change exacerbated the  
1260 exceptional 2022 European-Mediterranean drought. *Environ. Res. Lett.*, 18, 034030, DOI 10.1088/1748-  
1261 9326/acbc37, 2023  
1262  
1263 Fassbender, A. J., Alin, S. R., Feely, R. A., Sutton, A. J., Newton, J. A., Krembs, C., Bos, J., Keyzers, M., Devol,  
1264 A., Ruef, W., and Pelletier, G.: Seasonal carbonate chemistry variability in marine surface waters of the US  
1265 Pacific Northwest, *Earth Syst. Sci. Data*, 10, 1367–1401, <https://doi.org/10.5194/essd-10-1367-2018>, 2018.  
1266  
1267 Fay, A. R., and McKinley, G. A.: Global open-ocean biomes: Mean and temporal variability. *Earth System*  
1268 *Science Data*, 6(2), 273–284. <https://doi.org/10.5194/essd-6-273-2014>, 2014

1269  
1270 Fourrier, M., Coppola, L., Claustre, H., D'Ortenzio, F., Sauzède, R. and Gattuso, J.-P.: A regional neural  
1271 network approach to estimate water-column nutrient concentrations and carbonate system variables in the  
1272 Mediterranean Sea: CANYON-MED. *Frontiers in Marine Science*, 7:620,  
1273 <https://www.frontiersin.org/articles/10.3389/fmars.2020.00620>, 2020.  
1274  
1275 Friedlingstein, P., O'Sullivan, M., Jones, M. W., Andrew, R. M., Gregor, L., Hauck, J., Le Quéré, C., Luijkx, I.  
1276 T., Olsen, A., Peters, G. P., Peters, W., Pongratz, J., Schwingshackl, C., Sitch, S., Canadell, J. G., Ciais, P.,  
1277 Jackson, R. B., Alin, S. R., Alkama, R., Arneeth, A., Arora, V. K., Bates, N. R., Becker, M., Bellouin, N., Bittig,  
1278 H. C., Bopp, L., Chevallier, F., Chini, L. P., Cronin, M., Evans, W., Falk, S., Feely, R. A., Gasser, T., Gehlen,  
1279 M., Gkritzalis, T., Gloege, L., Grassi, G., Gruber, N., Gürses, Ö., Harris, I., Hefner, M., Houghton, R. A., Hurtt,  
1280 G. C., Iida, Y., Ilyina, T., Jain, A. K., Jersild, A., Kadono, K., Kato, E., Kennedy, D., Klein Goldewijk, K.,  
1281 Knauer, J., Korsbakken, J. I., Landschützer, P., Lefèvre, N., Lindsay, K., Liu, J., Liu, Z., Marland, G., Mayot, N.,  
1282 McGrath, M. J., Metzl, N., Monacchi, N. M., Munro, D. R., Nakaoka, S.-I., Niwa, Y., O'Brien, K., Ono, T.,  
1283 Palmer, P. I., Pan, N., Pierrot, D., Pocock, K., Poulter, B., Resplandy, L., Robertson, E., Rödenbeck, C.,  
1284 Rodriguez, C., Rosan, T. M., Schwinger, J., Séférian, R., Shutler, J. D., Skjelvan, I., Steinhoff, T., Sun, Q.,  
1285 Sutton, A. J., Sweeney, C., Takao, S., Tanhua, T., Tans, P. P., Tian, X., Tian, H., Tilbrook, B., Tsujino, H.,  
1286 Tubiello, F., van der Werf, G. R., Walker, A. P., Wanninkhof, R., Whitehead, C., Willstrand Wranne, A.,  
1287 Wright, R., Yuan, W., Yue, C., Yue, X., Zaehle, S., Zeng, J., and Zheng, B.: Global Carbon Budget 2022, *Earth*  
1288 *Syst. Sci. Data*, 14, 4811–4900, <https://doi.org/10.5194/essd-14-4811-2022>, 2022.  
1289  
1290 Friedlingstein, P., O'Sullivan, M., Jones, M. W., Andrew, R. M., Bakker, D. C. E., Hauck, J., Landschützer, P.,  
1291 Le Quéré, C., Luijkx, I. T., Peters, G. P., Peters, W., Pongratz, J., Schwingshackl, C., Sitch, S., Canadell, J. G.,  
1292 Ciais, P., Jackson, R. B., Alin, S. R., Anthoni, P., Barbero, L., Bates, N. R., Becker, M., Bellouin, N., Decharme,  
1293 B., Bopp, L., Brasika, I. B. M., Cadule, P., Chamberlain, M. A., Chandra, N., Chau, T.-T.-T., Chevallier, F.,  
1294 Chini, L. P., Cronin, M., Dou, X., Enyo, K., Evans, W., Falk, S., Feely, R. A., Feng, L., Ford, D. J., Gasser, T.,  
1295 Ghattas, J., Gkritzalis, T., Grassi, G., Gregor, L., Gruber, N., Gürses, Ö., Harris, I., Hefner, M., Heinke, J.,  
1296 Houghton, R. A., Hurtt, G. C., Iida, Y., Ilyina, T., Jacobson, A. R., Jain, A., Jarníková, T., Jersild, A., Jiang, F.,  
1297 Jin, Z., Joos, F., Kato, E., Keeling, R. F., Kennedy, D., Klein Goldewijk, K., Knauer, J., Korsbakken, J. I.,  
1298 Körtzinger, A., Lan, X., Lefèvre, N., Li, H., Liu, J., Liu, Z., Ma, L., Marland, G., Mayot, N., McGuire, P. C.,  
1299 McKinley, G. A., Meyer, G., Morgan, E. J., Munro, D. R., Nakaoka, S.-I., Niwa, Y., O'Brien, K. M., Olsen, A.,  
1300 Omar, A. M., Ono, T., Paulsen, M., Pierrot, D., Pocock, K., Poulter, B., Powis, C. M., Rehder, G., Resplandy, L.,  
1301 Robertson, E., Rödenbeck, C., Rosan, T. M., Schwinger, J., Séférian, R., Smallman, T. L., Smith, S. M.,  
1302 Sospedra-Alfonso, R., Sun, Q., Sutton, A. J., Sweeney, C., Takao, S., Tans, P. P., Tian, H., Tilbrook, B., Tsujino,  
1303 H., Tubiello, F., van der Werf, G. R., van Ooijen, E., Wanninkhof, R., Watanabe, M., Wimart-Rousseau, C.,  
1304 Yang, D., Yang, X., Yuan, W., Yue, X., Zaehle, S., Zeng, J., and Zheng, B.: Global Carbon Budget 2023, *Earth*  
1305 *Syst. Sci. Data*, 15, 5301–5369, <https://doi.org/10.5194/essd-15-5301-2023>, 2023.  
1306  
1307 Fröb, F., Olsen, A., Becker, M., Chafik, L., Johannessen, T., Reverdin, G., and Omar, A.: Wintertime fCO<sub>2</sub>  
1308 variability in the subpolar North Atlantic since 2004. *Geophysical Research Letters*, 46,  
1309 <https://doi.org/10.1029/2018GL080554>, 2019.  
1310  
1311 Gac, J.-P., Marrec, P., Cariou, T., Grosstefan, E., Macé, E., Rimmelin-Maury, P., Vernet, M., and Bozec, Y.:  
1312 Decadal Dynamics of the CO<sub>2</sub> System and Associated Ocean Acidification in Coastal Ecosystems of the North  
1313 East Atlantic Ocean. *Front. Mar. Sci.* 8:688008. doi:10.3389/fmars.2021.688008, 2021.  
1314  
1315 Gallego, M. A., Timmermann, A., Friedrich, T., and Zeebe, R. E.: Drivers of future seasonal cycle changes in  
1316 oceanic pCO<sub>2</sub>, *Biogeosciences*, 15, 5315–5327, <https://doi.org/10.5194/bg-15-5315-2018>, 2018.  
1317  
1318 Gattuso, J.-P., Magnan, A., Billé, R., Cheung, W. W. L., Howes, E. L., Joos, F., Allemand, D., Bopp, L., Cooley,  
1319 S., Eakin, M., Hoegh-Guldberg, O., Kelly, R. P., Pörtner, H.-O., Rogers, A. D., Baxter, J. M., Laffoley, D.,  
1320 Osborn, D., Rankovic, A., Rochette, J., Sumaila, U. R., Treyer, S., and Turley, C.: Contrasting futures for ocean

1321 and society from different anthropogenic CO<sub>2</sub> emissions scenarios. *Science* 349:aac4722.doi:  
1322 10.1126/science.aac4722, 2015.

1323

1324 Gattuso, Jean-Pierre; Alliouane, Samir; Mousseau, Laure (2021): Seawater carbonate chemistry in the Bay of  
1325 Villefranche, Point B (France), January 2007 - June 2023 [dataset]. PANGAEA,  
1326 <https://doi.org/10.1594/PANGAEA.727120>  
1327

1328 Gibb, O., Cyr, F., Azetsu-Scott, K., Chassé, J., Childs, D., Gabriel, C.-E., Galbraith, P. S., Maillet, G., Pepin, P.,  
1329 Punshon, S., and Starr, M.: Spatiotemporal variability in pH and carbonate parameters on the Canadian Atlantic  
1330 continental shelf between 2014 and 2022, *Earth Syst. Sci. Data*, 15, 4127–4162, <https://doi.org/10.5194/essd-15-4127-2023>, 2023.  
1331  
1332

1333 Goyet, C., Beauverger, C., Brunet, C., and Poisson, A.: Distribution of carbon dioxide partial pressure in surface  
1334 waters of the Southwest Indian Ocean, *Tellus B: Chemical and Physical Meteorology*, 43:1, 1-11, DOI:  
1335 [10.3402/tellusb.v43i1.15242](https://doi.org/10.3402/tellusb.v43i1.15242), 1991.  
1336

1337 Goyet C., Hassoun, A. E. R. Gemayel, E. Touratier, F., Abboud-Abi Saab M. and Guglielmi, V.:  
1338 Thermodynamic forecasts of the Mediterranean Sea Acidification. *Mediterranean Marine Science*, 17/2, 508-  
1339 518, <http://dx.doi.org/10.12681/mms.1487>, 2016  
1340

1341 Goyet C., Benallal, M.A., Bijoux A., Guglielmi, V., Moussa, H., Ribou, A.-C., and Touratier, F.: Ch.39,  
1342 Evolution of human Impact on Oceans: Tipping points of socio-ecological Coviability. In: *Coviability of Social  
1343 and Ecological Systems: Reconnecting Mankind to the Biosphere in an Era of Global Change*. O.Barrière et al.  
1344 (eds.) Springer International Publishing AG, part of Springer Nature 2019. [https://doi.org/10.1007/978-3-319-78111-2\\_12](https://doi.org/10.1007/978-3-319-78111-2_12), 2019  
1345  
1346

1347 Gregor, L. and Gruber, N.: OceanSODA-ETHZ: a global gridded data set of the surface ocean carbonate system  
1348 for seasonal to decadal studies of ocean acidification, *Earth Syst. Sci. Data*, 13, 777–808,  
1349 <https://doi.org/10.5194/essd-13-777-2021>, 2021.  
1350

1351 Gregor, L., Shutler, J., and Gruber, N.: High-resolution variability of the ocean carbon sink. *Global  
1352 Biogeochemical Cycles*, 38, e2024GB008127. <https://doi.org/10.1029/2024GB008127>, 2024  
1353

1354 Gruber, N., Clement, D. , Carter, B. R., Feely, R. A., van Heuven, S., Hoppema, M., Ishii, M., Key, R. M.,  
1355 Kozyr, A., Lauvset, S. K., Lo Monaco, C. , Mathis, J. T., Murata, A., Olsen, A., Perez, F. F., Sabine, C. L.,  
1356 Tanhua, T., and Wanninkhof, R.: The oceanic sink for anthropogenic CO<sub>2</sub> from 1994 to 2007, *Science* vol. 363  
1357 (issue 6432), pp. 1193-1199. DOI: 10.1126/science.aau5153, 2019.  
1358

1359 Guglielmi V., Touratier, F., and Goyet, C.: Design of sampling strategy measurements of CO<sub>2</sub>/carbonate  
1360 properties. *Journal of Oceanography and Aquaculture*, DOI: 10.23880/ijoac-16000227, 2022  
1361

1362 Guglielmi V., Touratier, F., and Goyet, C.: Determination of discrete sampling locations minimizing both the  
1363 number of samples and the maximum interpolation error: Application to measurements of carbonate chemistry in  
1364 surface ocean, *Journal of Sea Research*, <https://doi.org/10.1016/j.seares.2023.102336>, 2023  
1365

1366 Hauck, J., Gregor, L., Nissen, C., Patara, L., Hague, M., Mongwe, P., et al.: The Southern Ocean carbon cycle  
1367 1985–2018: Mean, seasonal cycle, trends, and storage. *Global Biogeochemical Cycles*, 37, e2023GB007848.  
1368 <https://doi.org/10.1029/2023GB007848>, 2023  
1369

1370 Ho, D. T., Bopp, L., Palter, J. B., Long, M. C., Boyd, P.W., Neukermans, G., and Bach, L. T. : Monitoring,  
1371 reporting, and verification for ocean alkalinity enhancement. *State of the Planet*, 2-oae2023, 1–12, 2023.  
1372



1373 Holliday, N.P., Bersch, M., Berx, B., Chafik, L., Cunningham, S., Florindo-López, C., Hátún, H., Johns, W.,  
1374 Josey, S.A., Larsen, K.M.H., Mulet, S., Oltmanns, M., Reverdin, G., Rossby, T., Thierry, V., Valdimarsson, H.,  
1375 Yashayev, I. : Ocean circulation causes the largest freshening event for 120 years in eastern subpolar North  
1376 Atlantic. *Nat. Commun.*, 11. <https://doi.org/10.1038/s41467-020-14474-y>, 2020  
1377  
1378 Howes, E., Stemmann, L., Assailly, C., Irisson, J.-O., Dima, M., Bijma, J., Gattuso, J.-P.: Pteropod time series  
1379 from the North Western Mediterranean (1967-2003): impacts of pH and climate variability. *Mar Ecol Prog Ser*  
1380 531: 193-206, doi: 10.3354/meps11322. 2015.  
1381  
1382 Huang, B., P. W. Thorne, V. F. Banzon, T. Boyer, G. Chepurin, J. H. Lawrimore, M. J. Menne, T. M. Smith, R.  
1383 S. Vose, and H.-M. Zhang: Extended Reconstructed Sea Surface Temperature, version 5 (ERSSTv5): Upgrades,  
1384 validations, and intercomparisons. *J. Climate*, 30, 8179-8205, doi:10.1175/JCLI-D-16-0836.1, 2017  
1385  
1386 IPCC. Changing Ocean, Marine Ecosystems, and Dependent Communities. in *The Ocean and Cryosphere in a*  
1387 *Changing Climate 447–588* (Cambridge University Press, 2022). doi:10.1017/9781009157964.007. 2022  
1388  
1389 Jiang, Z.-P., Tyrrell, T., Hydes, D. J., Dai, M., and Hartman, S. E.: Variability of alkalinity and the alkalinity-  
1390 salinity relationship in the tropical and subtropical surface ocean, *Global Biogeochem. Cycles*, 28, 729–742,  
1391 doi:10.1002/2013GB004678, 2014.  
1392  
1393 Jiang, L.-Q., Feely, R. A., Wanninkhof, R., Greeley, D., Barbero, L., Alin, S., Carter, B. R., Pierrot, D.,  
1394 Featherstone, C., Hooper, J., Melrose, C., Monacci, N., Sharp, J. D., Shellito, S., Xu, Y.-Y., Kozyr, A., Byrne, R.  
1395 H., Cai, W.-J., Cross, J., Johnson, G. C., Hales, B., Langdon, C., Mathis, J., Salisbury, J., and Townsend, D. W.:  
1396 Coastal Ocean Data Analysis Product in North America (CODAP-NA) – an internally consistent data product for  
1397 discrete inorganic carbon, oxygen, and nutrients on the North American ocean margins. *Earth System Science*  
1398 *Data*, 13(6), 2777–2799. <https://doi.org/10.5194/essd-13-2777-2021>, 2021  
1399  
1400 Jiang, L.-Q., Dunne, J., Carter, B. R., Tjiputra, J. F., Terhaar, J., Sharp, J. D., et al.: Global surface ocean  
1401 acidification indicators from 1750 to 2100. *Journal of Advances in Modeling Earth Systems*, 15,  
1402 e2022MS003563. <https://doi.org/10.1029/2022MS003563> , 2023  
1403  
1404 Jiang, L.Q., Fay, A., Müller, J. D. et al: Synthesis products for ocean carbon chemistry. In prep., 2024.  
1405  
1406 Jing, Y., Li, Y., Xu, Y., and Fan, G.: Influences of the NAO on the North Atlantic CO<sub>2</sub> fluxes in winter and  
1407 summer on the interannual scale. *Advances in Atmospheric Sciences*, 36(11), 1288–1298.  
1408 <https://doi.org/10.1007/s00376-019-8247-2>, 2019  
1409  
1410 Kapsenberg, L., Alliouane, S., Gazeau, F., Mousseau, L., and Gattuso, J.-P.: Coastal ocean acidification and  
1411 increasing total alkalinity in the northwestern Mediterranean Sea, *Ocean Sci.*, 13, 411-426, doi:10.5194/os-13-  
1412 411-2017, 2017.  
1413  
1414 Khatiwala, S., Tanhua, T., Mikaloff Fletcher, S., Gerber, M., Doney, S. C., Graven, H. D., Gruber, N.,  
1415 McKinley, G. A., Murata, A., Ríos, A. F., and Sabine, C. L.: Global ocean storage of anthropogenic carbon,  
1416 *Biogeosciences*, 10, 2169-2191, <https://doi.org/10.5194/bg-10-2169-2013>, 2013.  
1417  
1418 Koffi, U., Lefèvre, N., Kouadio, G., and Boutin, J.: Surface CO<sub>2</sub> parameters and air-sea CO<sub>2</sub> fluxes distribution  
1419 in the eastern equatorial Atlantic Ocean. *J. Marine Systems*, doi:10.1016/j.jmarsys/2010.04.010. 2010.  
1420  
1421 Kwiatkowski, L., Torres, O., Bopp, L., Aumont, O., Chamberlain, M., Christian, J. R., Dunne, J. P., Gehlen, M.,  
1422 Ilyina, T., John, J. G., Lenton, A., Li, H., Lovenduski, N. S., Orr, J. C., Palmieri, J., Santana-Falcón, Y.,  
1423 Schwinger, J., Séférian, R., Stock, C. A., Tagliabue, A., Takano, Y., Tjiputra, J., Toyama, K., Tsujino, H.,  
1424 Watanabe, M., Yamamoto, A., Yool, A., and Ziehn, T.: Twenty-first century ocean warming, acidification,

1425 deoxygenation, and upper-ocean nutrient and primary production decline from CMIP6 model projections,  
1426 Biogeosciences, 17, 3439–3470, <https://doi.org/10.5194/bg-17-3439-2020>, 2020.

1427

1428 Lacoue-Labarthe, T., Nunes, P. A. L. D., Ziveri, P., Cinar, M., Gazeau, F., Hall-Spencer, J. M., Hilmi, N.,  
1429 Moschella, P., Safa, A., Sauzade, D., and Turley, C.: Impacts of ocean acidification in a warming Mediterranean  
1430 Sea: An overview, *Regional Studies in Marine Science*, 5, 1–11, doi:10.1016/j.rsma.2015.12.005, 2016.

1431

1432 Lagoutte, E., A. Tribollet, S. Bureau, et al., Biogeochemical evidence of flow re-entrainment on the main  
1433 fringing reef of La Reunion Island, *Marine Chemistry*, <https://doi.org/10.1016/j.marchem.2024.104352>, 2023.

1434

1435 Laika, H. E., Goyet C., Vouve F., Poisson A., and Touratier F. : Interannual properties of the CO<sub>2</sub> system in the  
1436 Southern Ocean south of Australia. *Antarctic Science*, 21(6), 663–680.  
1437 <https://doi.org/10.1017/S0954102009990319>, 2009

1438

1439 Lan, X., Tans, P. and K.W. Thoning: Trends in globally-averaged CO<sub>2</sub> determined from NOAA Global  
1440 Monitoring Laboratory measurements. Version 2024-08 <https://doi.org/10.15138/9NOH-ZH07> (last access: 14  
1441 August 2024), 2024.

1442

1443 Landschützer, P., Gruber, N., Bakker, D. C. E., Stemmler, I., and Six, K. D.: Strengthening seasonal marine CO<sub>2</sub>  
1444 variations due to increasing atmospheric CO<sub>2</sub>. *Nature Climate Change*, 8(2), 146–150.  
1445 <https://doi.org/10.1038/s41558-017-0057-x>, 2018

1446

1447 Landschützer, P., Ilyina, T., and Lovenduski, N. S. : Detecting regional modes of variability in observation-  
1448 based surface ocean pCO<sub>2</sub>. *Geophysical Research Letters*, 46. <https://doi.org/10.1029/2018GL081756>, 2019

1449

1450 Lange, N., Fiedler, B., Álvarez, M., Benoit-Cattin, A., Benway, H., Buttigieg, P. L., Coppola, L., Currie, K.,  
1451 Flecha, S., Gerlach, D. S., Honda, M., Huertas, I. E., Lauvset, S. K., Muller-Karger, F., Körtzinger, A., O'Brien,  
1452 K. M., Ólafsdóttir, S. R., Pacheco, F. C., Rueda-Roa, D., Skjelvan, I., Wakita, M., White, A., and Tanhua, T.:  
1453 Synthesis Product for Ocean Time Series (SPOTS) – a ship-based biogeochemical pilot, *Earth Syst. Sci. Data*,  
1454 16, 1901–1931, <https://doi.org/10.5194/essd-16-1901-2024>, 2024.

1455

1456 LANSARD Bruno (2014) DICASE cruise, RV Téthys II, <https://doi.org/10.17600/14007100>

1457

1458 Laruelle, G. G., Dürr, H. H., Lauerwald, R., Hartmann, J., Slomp, C. P., Goossens, N., and Regnier, P. A. G.:  
1459 Global multi-scale segmentation of continental and coastal waters from the watersheds to the continental  
1460 margins, *Hydrol. Earth Syst. Sci.*, 17, 2029–2051, <https://doi.org/10.5194/hess-17-2029-2013>, 2013.

1461

1462 Laruelle, G. G. et al. Continental shelves as a variable but increasing global sink for atmospheric carbon dioxide.  
1463 *Nat. Commun.* 9, 454, DOI: 10.1038/s41467-017-02738-z, 2018

1464

1465 Lauvset, S. K., Lange, N., Tanhua, T., Bittig, H. C., Olsen, A., Kozyr, A., Álvarez, M., Azetsu-Scott, K., Brown,  
1466 P. J., Carter, B. R., Cotrim da Cunha, L., Hoppema, M., Humphreys, M. P., Ishii, M., Jeansson, E., Murata, A.,  
1467 Müller, J. D., Pérez, F. F., Schirnick, C., Steinfeldt, R., Suzuki, T., Ulfsbo, A., Velo, A., Woosley, R. J., and  
1468 Key, R. M.: The annual update GLODAPv2.2023: the global interior ocean biogeochemical data product, *Earth*  
1469 *Syst. Sci. Data*, 16, 2047–2072, <https://doi.org/10.5194/essd-16-2047-2024>, 2024.

1470

1471 Lefèvre, D.: MOOSE (ANTARES), <https://doi.org/10.18142/233>, 2010.

1472

1473 Lefèvre N.: Carbon parameters along a zonal transect. SEANOE. <https://doi.org/10.17882/58575>, 2010.

1474

1475 Lefèvre Nathalie (2017). Carbon parameters in the gulf of Maranhao. SEANOE. <https://doi.org/10.17882/62417>

1476

1477 Lefèvre Nathalie (2018). Carbon parameters in the Western tropical Atlantic. SEANOE.  
1478 <https://doi.org/10.17882/58406>  
1479

1480 Lefèvre Nathalie (2019). Carbon parameters in the Eastern Tropical Atlantic in 2019. SEANOE.  
1481 <https://doi.org/10.17882/83682>  
1482

1483 Lefèvre Nathalie (2020). Inorganic carbon and alkalinity in the Eastern tropical Atlantic measured during the  
1484 PIRATA FR-30 cruise in February-March 2020. SEANOE. <https://doi.org/10.17882/90742>  
1485

1486 Lefèvre Nathalie (2022). Inorganic carbon and alkalinity in the Eastern tropical Atlantic in 2022. SEANOE.  
1487 <https://doi.org/10.17882/92386>  
1488

1489 Lefèvre, N., Urbano, D.F., Gallois, F., and Diverrès, D.: Impact of physical processes on the seasonal  
1490 distribution of CO<sub>2</sub> in the western tropical Atlantic. *Journal of Geophysical Research* 119,  
1491 doi: 10.1002/2013JC009248. doi: DOI: 10.1002/2013JC009248, 2014  
1492

1493 Lefèvre, N., Veleda, D., Araujo, M., Caniaux, G.: Variability and trends of carbon parameters at a time series in  
1494 the eastern tropical Atlantic. *Tellus B*, Co-Action Publishing, 68, pp.30305. 10.3402/tellusb.v68.30305. 2016.  
1495

1496 Lefèvre N., da Silva Dias F. J., de Torres A. R., Noriega C., Araujo M., de Castro A. C. L., Rocha C., Jiang S.,  
1497 Ibánhez J. S. P.: A source of CO<sub>2</sub> to the atmosphere throughout the year in the Maranhense continental shelf  
1498 (2°30'S, Brazil). *Continental Shelf Research*, 141, 38-50. <https://doi.org/10.1016/j.csr.2017.05.004>, 2017a  
1499

1500 Lefèvre N., Flores Montes M., Gaspar F. L., Rocha C., Jiang S., De Araújo M. C., Ibánhez J. S. P.: Net  
1501 Heterotrophy in the Amazon Continental Shelf Changes Rapidly to a Sink of CO<sub>2</sub> in the Outer Amazon Plume.  
1502 *Frontiers in Marine Science*, 4, -. <https://doi.org/10.3389/fmars.2017.00278>, 2017b  
1503

1504 Lefèvre, N., Mejia, C., Khvorostyanov, D., Beaumont, L., and Koffi, U.: Ocean Circulation Drives the  
1505 Variability of the Carbon System in the Eastern Tropical Atlantic. *Oceans*, 2021, 2, 126–148.  
1506 <https://doi.org/10.3390/oceans2010008>, 2021.  
1507

1508 Lefèvre, N., Veleda, D., Hartman, S.E.: Outgassing of CO<sub>2</sub> dominates in the coastal upwelling off the northwest  
1509 African coast, *Deep-Sea Research Part I*, doi: <https://doi.org/10.1016/j.dsr.2023.104130>, 2023  
1510

1511 Lefèvre, N., Veleda, D. and Beaumont; L.: Trends and drivers of CO<sub>2</sub> parameters, from 2006 to 2021, at a time-  
1512 series station in the Eastern Tropical Atlantic (6°S, 10°W). *Front. Mar. Sci.* 11:1299071. doi:  
1513 10.3389/fmars.2024.1299071, 2024  
1514

1515 Leseurre, C.: Mécanismes de contrôle de l'absorption de CO<sub>2</sub> anthropique et de l'acidification des eaux dans les  
1516 océans Atlantique Nord et Austral. PhD Thesis, Sorbonne Univ., 270 pp. <https://theses.hal.science/tel-04028410>,  
1517 2022  
1518

1519 Leseurre, C., Lo Monaco, C., Reverdin, G., Metzl, N., Fin, J., Olafsdottir, S., and Racapé, V.: Ocean carbonate  
1520 system variability in the North Atlantic Subpolar surface water (1993–2017), *Biogeosciences*, 17, 2553–2577,  
1521 <https://doi.org/10.5194/bg-17-2553-2020>, 2020  
1522

1523 Leseurre, C., Lo Monaco, C., Reverdin, G., Metzl, N., Fin, J., Mignon, C., and Benito, L.: Summer trends and  
1524 drivers of sea surface fCO<sub>2</sub> and pH changes observed in the southern Indian Ocean over the last two decades  
1525 (1998–2019), *Biogeosciences*, 19, 2599–2625, <https://doi.org/10.5194/bg-19-2599-2022>, 2022.  
1526

1527 Li, X., et al.: The source and accumulation of anthropogenic carbon in the U.S. East Coast, *Sci. Adv.* 10,  
1528 ead13169, DOI: 10.1126/sciadv.ad13169, 2024  
1529



1530 LO MONACO Claire, METZL Nicolas (2019) VT 163 / OISO-29 cruise, RV Marion Dufresne,  
1531 <https://doi.org/10.17600/18000972>  
1532  
1533 LO MONACO Claire (2020) OISO-30 cruise, RV Marion Dufresne, <https://doi.org/10.17600/18000679>  
1534  
1535 LO MONACO Claire, JEANDEL Catherine, PLANQUETTE H el ene (2021) OISO-31 cruise, RV Marion  
1536 Dufresne, <https://doi.org/10.17600/18001254>  
1537  
1538 Lo Monaco, Claire; Metzl, Nicolas; Fin, Jonathan (2022). Sea surface measurements of dissolved inorganic  
1539 carbon (DIC), total alkalinity (TALK), temperature and salinity during the R/V Marion-Dufresne Ocean Indien  
1540 Service d'Observations - 29 (OISO-29) cruise (EXPOCODE 35MV20190106) in the Indian Ocean from 2019-  
1541 01-06 to 2019-02-09 (NCEI Accession 0252612). NOAA National Centers for Environmental Information.  
1542 Dataset. <https://doi.org/10.25921/8ajx-za24>. Accessed 14-Aug-2024.  
1543  
1544 Lo Monaco, Claire; Metzl, Nicolas (2023). Sea surface measurements of dissolved inorganic carbon (DIC), total  
1545 alkalinity (TALK), temperature and salinity during the R/V Marion-Dufresne Ocean Indien Service  
1546 d'Observations - 30 (OISO-30) cruise (EXPOCODE 35MV20200106) in the Indian Ocean from 2020-01-06 to  
1547 2020-02-01 (NCEI Accession 0280937). NOAA National Centers for Environmental Information. Dataset.  
1548 <https://doi.org/10.25921/n2g0-pp38>. Accessed 14-Aug-2024  
1549  
1550 Lo Monaco, Claire; Metzl, Nicolas; Fin, Jonathan (2023). Sea surface measurements of dissolved inorganic  
1551 carbon (DIC), total alkalinity (TALK), temperature and salinity during the R/V Marion-Dufresne Ocean  
1552 Indien Service d'Observations - 31 (OISO-31) cruise (EXPOCODE 35MV20210113) in the Indian Ocean  
1553 from 2021-01-14 to 2021-03-04 (NCEI Accession 0280946). NOAA National Centers for Environmental  
1554 Information. Dataset. <https://doi.org/10.25921/7sb2-k852>. Accessed 14-Aug-2024  
1555  
1556 Mathis, M., Lacroix, F., Hagemann, S. et al.: Enhanced CO2 uptake of the coastal ocean is dominated by  
1557 biological carbon fixation. *Nat. Clim. Chang.* <https://doi.org/10.1038/s41558-024-01956-w>, 2024  
1558  
1559 Maugendre, L., J.-P. Gattuso, J. Louis, A. de Kluijver, S. Marro, K. Soetaert, F. Gazeau: Effect of ocean  
1560 warming and acidification on a plankton community in the NW Mediterranean Sea, *ICES Journal of Marine*  
1561 *Science*, Volume 72, Issue 6, July/August 2015, Pages 1744–1755, <https://doi.org/10.1093/icesjms/fsu161>, 2015  
1562  
1563 Mercier, H., Lherminier, P., Sarafanov, A., Gaillard, F., Daniault, N., Desbry eres, D., Falina, A., Ferron, B.,  
1564 Huck, T., and Thierry, V.: Variability of the meridional overturning circulation at the Greenland-Portugal Ovide  
1565 section from 1993 to 2010. *Progress in Oceanography*, 132, 250-261, [doi:10.1016/j.pocean.2013.11.001](https://doi.org/10.1016/j.pocean.2013.11.001). 2015  
1566  
1567 Mercier, H., Desbry eres, D., Lherminier, P., Velo, A., Carracedo, L., Fontela, M., and P erez, F. F.: New  
1568 insights into the eastern subpolar North Atlantic meridional overturning circulation from OVIDE, *Ocean Sci.*,  
1569 20, 779–797, <https://doi.org/10.5194/os-20-779-2024>, 2024.  
1570  
1571 Metzl, N., Brunet, C., Jabaud-Jan, A., Poisson, A., and Schauer, B.: Summer and winter air-sea CO2 fluxes in  
1572 the Southern Ocean *Deep Sea Res I*, 53, 1548-1563, [doi:10.1016/j.dsr.2006.07.006](https://doi.org/10.1016/j.dsr.2006.07.006). 2006.  
1573  
1574 Metzl, N., Corbi ere, A., Reverdin, G., Lenton, A., Takahashi, T., Olsen, A., Johannessen, T., Pierrot, D.,  
1575 Wanninkhof, R.,  lafsd ottir, S. R., Olafsson, J., and Ramonet, M.: Recent acceleration of the sea surface fCO2  
1576 growth rate in the North Atlantic subpolar gyre (1993-2008) revealed by winter observations, *Global*  
1577 *Biogeochem. Cycles*, 24, GB4004, [doi:10.1029/2009GB003658](https://doi.org/10.1029/2009GB003658), 2010.  
1578  
1579 Metzl, N., and Lo Monaco, C.: OISO - OC EAN INDIEN SERVICE D'OBSERVATION,  
1580 <https://doi.org/10.18142/228>, 1998.  
1581

1582 Metz, N., Lo Monaco, C., Leseurre, C., Ridame, C., Fin, J., Mignon, C., Gehlen, M., and Chau, T. T. T.: The  
1583 impact of the South-East Madagascar Bloom on the oceanic CO<sub>2</sub> sink, *Biogeosciences*, 19, 1451–1468,  
1584 <https://doi.org/10.5194/bg-19-1451-2022>, 2022  
1585

1586 Metz, N., Fin, J., Lo Monaco, C., Mignon, C., Alliouane, S., Antoine, D., Bourdin, G., Boutin, J., Bozec, Y.,  
1587 Guillaume, G., Boutin, J., Bozec, Y., Conan, P., Coppola, L., Diaz, F., Douville, E., Durrieu de Madron, X.,  
1588 Gattuso, J.-P., Gazeau, F., Golbol, M., Lansard, B., Lefèvre, D., Lefèvre, N., Lombard, F., Louanchi, F.,  
1589 Merlivat, L., Olivier, L., Petrenko, A., Petton, S., Pujo-Pay, M., Rabouille, C., Reverdin, G.,  
1590 Ridame, C., Tribollet, A., Vellucci, V., Wagener, T., and Wimart-Rousseau, C.: A synthesis of ocean total  
1591 alkalinity and dissolved inorganic carbon observations in the global ocean (1993–2022). *SEANOE*.  
1592 <https://doi.org/10.17882/95414>, 2023  
1593  
1594

1595 Metz, N., Fin, J., Lo Monaco, C., Mignon, C., Alliouane, S., Antoine, D., Bourdin, G., Boutin, J., Bozec, Y.,  
1596 Conan, P., Coppola, L., Diaz, F., Douville, E., Durrieu de Madron, X., Gattuso, J.-P., Gazeau, F., Golbol, M.,  
1597 Lansard, B., Lefèvre, D., Lefèvre, N., Lombard, F., Louanchi, F., Merlivat, L., Olivier, L., Petrenko, A.,  
1598 Petton, S., Pujo-Pay, M., Rabouille, C., Reverdin, G., Ridame, C., Tribollet, A., Vellucci, V., Wagener, T.,  
1599 and Wimart-Rousseau, C.: A synthesis of ocean total alkalinity and dissolved inorganic carbon measurements  
1600 from 1993 to 2022: the SNAPO-CO<sub>2</sub>-v1 dataset, *Earth Syst. Sci. Data*, 16, 89–120, <https://doi.org/10.5194/essd-16-89-2024>,  
1601 2024a  
1602

1603 Metz, N., Lo Monaco, C., Leseurre, C., Ridame, C., Reverdin, G., Chau, T. T. T., Chevallier, F., and Gehlen,  
1604 M.: Anthropogenic CO<sub>2</sub>, air–sea CO<sub>2</sub> fluxes, and acidification in the Southern Ocean: results from a time-series  
1605 analysis at station OISO-KERFIX (51° S–68° E), *Ocean Sci.*, 20, 725–758, [https://doi.org/10.5194/os-20-725-](https://doi.org/10.5194/os-20-725-2024)  
1606 2024, 2024b.  
1607

1608 Metz, N., Lo Monaco, C., Barut, G., and TERNON, J.-F.: Contrasting trends of the ocean CO<sub>2</sub> sink and pH in the  
1609 Agulhas current system and the Mozambique Basin, South-Western Indian Ocean (1963–2023). *Deep Sea Res.*,  
1610 special issue IIOE-2, in rev., 2024c  
1611

1612 Metz, N., Fin, J., Lo Monaco, C., Mignon, C., Alliouane, S., Bombled, B., Boutin, J., Bozec, Y., Comeau,  
1613 S., Conan, P., Coppola, L., Cuet, P., Ferreira, E., Gattuso, J.-P., Gazeau, F., Goyet, C., Grossteffan, E.,  
1614 Lansard, B., Lefèvre, D., Lefèvre, N., Lombard, F., Louanchi, F., Merlivat, L., Olivier, L., Petrenko, A.,  
1615 Petton, S., Pujo-Pay, M., Rabouille, C., Reverdin, G., Ridame, C., Rimmelin, M., TERNON, J.-F., Touratier,  
1616 F., Tribollet, A., Wagener, T., and Wimart-Rousseau, C.: An updated synthesis of ocean total alkalinity and  
1617 dissolved inorganic carbon measurements from 1993 to 2023: the SNAPO-CO<sub>2</sub>-v2 dataset. *SEANOE*.  
1618 <https://doi.org/10.17882/102337>, 2024d  
1619

1620 MICHEL, E., and VIVIER, F.: STEP 2016 cruise, RV L'Atalante, <https://doi.org/10.17600/16000900>,  
1621 2016  
1622

1623 Mu, L., Gomes, H. do R., Burns, S. M., Goes, J. I., Coles, V. J., Rezende, C. E., et al.: Temporal Variability of  
1624 Air-Sea CO<sub>2</sub> flux in the Western Tropical North Atlantic Influenced by the Amazon River Plume. *Global  
1625 Biogeochemical Cycles*, 35(6). <https://doi.org/10.1029/2020GB006798>, 2021  
1626

1627 Munro, D. R., Lovenduski, N. S., Takahashi, T., Stephens, B. B., Newberger, T., and Sweeney, C.: Recent  
1628 evidence for a strengthening CO<sub>2</sub> sink in the Southern Ocean from carbonate system measurements in the Drake  
1629 Passage (2002–2015), *Geophys. Res. Lett.*, 42, 7623–7630, <https://doi.org/10.1002/2015GL065194>, 2015.  
1630

1631 Müller, J. D., Gruber, N., Carter, B., Feely, R., Ishii, M., Lange, N., et al.: Decadal trends in the oceanic storage  
1632 of anthropogenic carbon from 1994 to 2014. *AGU Advances*, 4, e2023AV000875.  
1633 <https://doi.org/10.1029/2023AV000875>, 2023  
1634

1635  
1636 Newton, J.A., Feely, R. A., Jewett, E. B., Williamson, P. and Mathis, J.: Global Ocean Acidification Observing  
1637 Network: Requirements and Governance Plan. Second Edition, GOA-ON,  
1638 <https://www.iaea.org/sites/default/files/18/06/goa-on-second-edition-2015.pdf>, 2015.  
1639  
1640 Olafsson, J., Olafsdottir, S. R., Benoit-Cattin, A., and Takahashi, T.: The Irminger Sea and the Iceland Sea time  
1641 series measurements of sea water carbon and nutrient chemistry 1983–2008, *Earth Syst. Sci. Data*, 2, 99–104,  
1642 <https://doi.org/10.5194/essd-2-99-2010>, 2010.  
1643  
1644 Olivier, L., Boutin, J., Reverdin, G., Lefèvre, N., Landschützer, P., Speich, S., Karstensen, J., Labaste, M.,  
1645 Noisel, C., Ritschel, M., Steinhoff, T., and Wanninkhof, R.: Wintertime process study of the North Brazil  
1646 Current rings reveals the region as a larger sink for CO<sub>2</sub> than expected, *Biogeosciences*, 19, 2969–2988,  
1647 <https://doi.org/10.5194/bg-19-2969-2022>, 2022.  
1648  
1649 Olsen, A., Key, R. M., van Heuven, S., Lauvset, S. K., Velo, A., Lin, X., Schirnick, C., Kozyr, A., Tanhua, T.,  
1650 Hoppema, M., Jutterström, S., Steinfeldt, R., Jeansson, E., Ishii, M., Pérez, F. F., and Suzuki, T.: The Global  
1651 Ocean Data Analysis Project version 2 (GLODAPv2) – an internally consistent data product for the world ocean,  
1652 *Earth Syst. Sci. Data*, 8, 297–323, <https://doi.org/10.5194/essd-8-297-2016>, 2016.  
1653  
1654 Oudot, C., Ternon, J. F., and Lecomte, J.: Measurements of atmospheric and oceanic CO<sub>2</sub> in the tropical Atlantic:  
1655 10 years after the 1982–1984 FOCAL cruises. *Tellus B: Chemical and Physical Meteorology*, 47(1–2), 70–85.  
1656 <https://doi.org/10.3402/tellusb.v47i1-2.16032>, 1995  
1657  
1658 Padin, X. A., Velo, A., and Pérez, F. F.: ARIOS: a database for ocean acidification assessment in the Iberian  
1659 upwelling system (1976–2018), *Earth Syst. Sci. Data*, 12, 2647–2663, [https://doi.org/10.5194/essd-12-2647-](https://doi.org/10.5194/essd-12-2647-2020)  
1660 2020, 2020.  
1661  
1662 Palacio-Castro, A. M., Enochs, I. C., Besemer, N., Boyd, A., Jankulak, M., Kolodziej, G., et al.: Coral reef  
1663 carbonate chemistry reveals interannual, seasonal, and spatial impacts on ocean acidification off Florida. *Global*  
1664 *Biogeochemical Cycles*, 37, e2023GB007789. <https://doi.org/10.1029/2023GB007789>, 2023  
1665  
1666 Pardo, P. C., Tilbrook, B., Langlais, C., Trull, T. W., and Rintoul, S. R.: Carbon uptake and biogeochemical  
1667 change in the Southern Ocean, south of Tasmania. *Biogeosciences*, 14(22), 5217–5237.  
1668 <https://doi.org/10.5194/bg-14-5217-2017>, 2017.  
1669  
1670 Pérez, F. F., Becker, M., Goris, N., Gehlen, M., López-Mozos, M., Tjiputra, J., et al.: An assessment of CO<sub>2</sub>  
1671 storage and sea-air fluxes for the Atlantic Ocean and Mediterranean Sea between 1985 and 2018. *Global*  
1672 *Biogeochemical Cycles*, 38, e2023GB007862. <https://doi.org/10.1029/2023GB007862>, 2024  
1673  
1674 Petton, S., Pernet, F., Le Roy, V., Huber, M., Martin, S., Macé, É., Bozec, Y., Loisel, S., Rimmelin Maury, P.,  
1675 Grossteffan, É., Repecaud, M., Quemener, L., Retho, M., Manac'h, S., Papin, M., Pineau, P., Lacoue-Labarthe,  
1676 T., Deborde, J., Costes, L., Polsenaere, P., Rigouin, L., Benhamou, J., Gouriou, L., Lequeux, J., Labourdette, N.,  
1677 Savoye, N., Messiaen, G., Foucault, E., Ouisse, V., Richard, M., Lagarde, F., Voron, F., Kempf, V., Mas, S.,  
1678 Giannecchini, L., Vidussi, F., Mostajir, B., Leredde, Y., Alliouane, S., Gattuso, J.-P., and Gazeau, F.: French  
1679 coastal network for carbonate system monitoring: the CocoriCO<sub>2</sub> dataset, *Earth Syst. Sci. Data*, 16, 1667–1688,  
1680 <https://doi.org/10.5194/essd-16-1667-2024>, 2024.  
1681  
1682 Petton Sébastien, Pernet Fabrice, Le Roy Valerian, Huber Matthias, Martin Sophie, Mace Eric, Bozec Yann,  
1683 Loisel Stéphane, Rimmelin-Maury Peggy, Grossteffan Emilie, Repecaud Michel, Quémener Loïc, Retho  
1684 Michael, Manach Soazig, Papin Mathias, Pineau Philippe, Lacoue-Labarthe Thomas, Deborde Jonathan, Costes  
1685 Louis, Polsenaere Pierre, Rigouin Loic, Benhamou Jeremy, Gouriou Laure, Lequeux Joséphine, Labourdette  
1686 Nathalie, Savoye Nicolas, Messiaen Gregory, Foucault Elodie, Lagarde Franck, Richard Marion, Ouisse  
1687 Vincent, Voron Florian, Mas Sébastien, Giannecchini Léa, Vidussi Francesca, Mostajir Behzad, Leredde Yann,

1688 Kempf Valentin, Alliouane Samir, Gattuso Jean-Pierre, Gazeau Frédéric: French coastal carbonate dataset from  
1689 the CocoriCO2 project. SEANO. <https://doi.org/10.17882/96982>, 2023  
1690  
1691 Poisson, A., Culkin, F., and Ridout, P.: Intercomparison of CO2 measurements. Deep Sea Research Part A.  
1692 Oceanographic Research Papers, 37, 10, 1647-1650, [https://doi.org/10.1016/0198-0149\(90\)90067-6](https://doi.org/10.1016/0198-0149(90)90067-6), 1990.  
1693  
1694 Pozzato, L., Rassmann, J., Lansard, B., Dumoulin, J.-P., Van Breugel, P., and Rabouille, C.: Origin of  
1695 remineralized organic matter in sediments from the Rhone River prodelta (NW Mediterranean) traced by Delta  
1696 C-14 and delta C-13 signatures of pore water DIC. Progress In Oceanography, 163, 112-122.  
1697 <https://doi.org/10.1016/j.pocean.2017.05.008>, 2018  
1698  
1699 RABOUILLE Christophe (2010) MESURHOBENT 1 cruise, RV Téthys II, <https://doi.org/10.17600/10450020>  
1700  
1701 RABOUILLE Christophe (2013) CARBODELTA cruise, RV Téthys II, <https://doi.org/10.17600/13450060>  
1702  
1703 RABOUILLE Christophe (2018) MISSRHODIA2 cruise, RV Téthys II, <https://doi.org/10.17600/18000473>  
1704  
1705 RABOUILLE Christophe, BOURRIN François, BASSETTI Maria-Angela (2022) DELTARHONE-1 cruise, RV  
1706 Téthys II, <https://doi.org/10.17600/18002027>  
1707  
1708 Regnier, P., Friedlingstein, P., Ciais, P., Mackenzie, F. T., Gruber, N., et al: Anthropogenic perturbation of the  
1709 carbon fluxes from land to ocean. Nat. Geosci. 6:597–607, 2013.  
1710  
1711 Resplandy, L., Hogikyan, A., Müller, J. D., Najjar, R. G., Bange, H. W., Bianchi, D., et al.: A synthesis of global  
1712 coastal ocean greenhouse gas fluxes. Global Biogeochemical Cycles, 38, e2023GB007803.  
1713 <https://doi.org/10.1029/2023GB007803>, 2024  
1714  
1715 Revelle, R., and Suess, H. E.: Carbon dioxide exchange between atmosphere and ocean and the question of an  
1716 increase of atmospheric CO2 during the past decades. Tellus 9, 18–27. doi:10.1111/j.2153-  
1717 3490.1957.tb01849.x., 1957.  
1718  
1719 Reverdin, G., Metzl, N., Olafsdottir, S., Racapé, V., Takahashi, T., Benetti, M., Valdimarsson, H., Benoit-Cattin,  
1720 A., Danielsen, M., Fin, J., Naamar, A., Pierrot, D., Sullivan, K., Bringas, F., and Goni, G.: SURATLANT: a  
1721 1993–2017 surface sampling in the central part of the North Atlantic subpolar gyre, Earth Syst. Sci. Data, 10,  
1722 1901-1924, <https://doi.org/10.5194/essd-10-1901-2018>, 2018.  
1723  
1724 Reverdin, G., Metzl, N., Olafsdottir, S., Racapé, V., Takahashi, T., Benetti, M., Valdimarsson, H., Quay, P. D.,  
1725 Benoit-Cattin, A., Danielsen, M., Fin, J., Naamar, A., Pierrot, D., Sullivan, K., Bringas, F., Goni, G., Becker M.,  
1726 Leseurre C., and Olsen A.: SURATLANT: a surface dataset in the central part of the North Atlantic subpolar  
1727 gyre. SEANO. <https://doi.org/10.17882/54517>, 2023.  
1728  
1729 Rodgers, K. B., Schwinger, J., Fassbender, A. J., Landschützer, P., Yamaguchi, R., Frenzel, H., et al.: Seasonal  
1730 variability of the surface ocean carbon cycle: A synthesis. Global Biogeochemical Cycles, 37, e2023GB007798.  
1731 <https://doi.org/10.1029/2023GB007798>, 2023  
1732  
1733 Roobaert, A., Resplandy, L., Laruelle, G. G., Liao, E., and Regnier, P. : Unraveling the physical and biological  
1734 controls of the global coastal CO2 sink. Global Biogeochemical Cycles, 38, e2023GB007799.  
1735 <https://doi.org/10.1029/2023GB007799>, 2024a  
1736  
1737 Roobaert, A., Regnier, P., Landschützer, P., and Laruelle, G. G.: A novel sea surface pCO2-product for the  
1738 global coastal ocean resolving trends over 1982–2020, Earth Syst. Sci. Data, 16, 421–441,  
1739 <https://doi.org/10.5194/essd-16-421-2024>, 2024b.  
1740

1741 Sarma, V. V. S. S., Krishna, M. S., Paul, Y. S., and Murty, V. S. N.: Observed changes in ocean acidity and  
1742 carbon dioxide exchange in the coastal bay of Bengal—A link to air pollution. *Tellus B: Chemical and Physical*  
1743 *Meteorology*, 67(1), 24638. <https://doi.org/10.3402/tellusb.v67.24638>, 2015  
1744  
1745 Sarma, V. V. S. S., Sridevi, B., Metzl, N., Patra, P. K., Lachkar, Z., Chakraborty, K., et al. : Air-sea fluxes of  
1746 CO<sub>2</sub> in the Indian Ocean between 1985 and 2018: A synthesis based on observation-based surface CO<sub>2</sub>, hindcast  
1747 and atmospheric inversion models. *Global Biogeochemical Cycles*, 37, e2023GB007694.  
1748 <https://doi.org/10.1029/2023GB007694>, 2023  
1749  
1750 Sarmiento, J.L., Johnson, K.S., Arteaga, L.A., Bushinsky, S.M., Cullen, H.M., Gray, A.R., Hotinski, R.M.,  
1751 Maurer, T.L., Mazloff, M.R., Riser, S.C., Russell, J.L., Schofield, O.M., Talley, L.D., The Southern Ocean  
1752 Carbon and Climate Observations and Modeling (SOCCOM) project: A review, *Progress in Oceanography*, doi:  
1753 <https://doi.org/10.1016/j.pocean.2023.103130>, 2023  
1754  
1755 Schlitzer, R.: Ocean Data View, Ocean Data View, <http://odv.awi.de> (last access: 13 March 2019), 2018.  
1756  
1757 Schneider, A., Wallace, D. W. R., and Körtzinger, A.: Alkalinity of the Mediterranean Sea, *Geophys. Res. Lett.*,  
1758 34, L15608, doi:10.1029/2006GL028842, 2007.  
1759  
1760 Schuster, U., McKinley, G. A., Bates, N., Chevallier, F., Doney, S. C., Fay, A. R., González-Dávila, M., Gruber,  
1761 N., Jones, S., Krijnen, J., Landschützer, P., Lefèvre, N., Manizza, M., Mathis, J., Metzl, N., Olsen, A., Rios, A.  
1762 F., Rödenbeck, C., Santana-Casiano, J. M., Takahashi, T., Wanninkhof, R., and Watson, A. J.: An assessment of  
1763 the Atlantic and Arctic sea–air CO<sub>2</sub> fluxes, 1990–2009, *Biogeosciences*, 10, 607–627,  
1764 <https://doi.org/10.5194/bg-10-607-2013>, 2013.  
1765  
1766 Shadwick, E., Rintoul, S., Tilbrook, B., Williams, G., Young, N., Fraser, A. D., et al.: Glacier tongue calving  
1767 reduced dense water formation and enhanced carbon uptake. *Geophysical Research Letters*, 40(5), 904–909.  
1768 <https://doi.org/10.1002/grl.50178>, 2013  
1769  
1770 Shadwick, E. H., B. Tilbrook, and G. D. Williams: Carbonate chemistry in the Mertz Polynya (East Antarctica):  
1771 Biological and physical modification of dense water outflows and the export of anthropogenic CO<sub>2</sub>, *J. Geophys.*  
1772 *Res. Oceans*, 119, 1–14, doi:10.1002/2013JC009286, 2014  
1773  
1774 Shadwick, E. H., T. W. Trull, B. Tilbrook, A. J. Sutton, E. Schulz, and C. L. Sabine: Seasonality of biological  
1775 and physical controls on surface ocean CO<sub>2</sub> from hourly observations at the Southern Ocean Time Series site  
1776 south of Australia, *Global Biogeochem. Cycles*, 29, 223–238, doi:10.1002/2014GB004906, 2015  
1777  
1778 Shadwick, E. H., Wynn-Edwards, C. A., Matear, R. J., Jansen, P., Schulz, E. and Sutton, A. J.: Observed  
1779 amplification of the seasonal CO<sub>2</sub> cycle at the Southern Ocean Time Series. *Front. Mar. Sci.* 10:1281854. doi:  
1780 10.3389/fmars.2023.1281854, 2023  
1781  
1782 Siddiqui, A. H., Haine, T. W. N., Nguyen, A. T., and Buckley, M. W.: Controls on upper ocean salinity  
1783 variability in the eastern subpolar North Atlantic during 1992–2017. *Journal of Geophysical*  
1784 *Research: Oceans*, 129, e2024JC020887. <https://doi.org/10.1029/2024JC020887>, 2024  
1785  
1786 Sridevi, B., and Sarma, V. V. S. S.: Role of river discharge and warming on ocean acidification and pco<sub>2</sub> levels  
1787 in the Bay of Bengal. *Tellus B: Chemical and Physical Meteorology*, 73 (1), 1–20., DOI:  
1788 10.1080/16000889.2021.1971924, 2021  
1789  
1790 Sutton, A.J., Battisti, R., Carter, B., Evans, W., Newton, J., Alin, S., Bates, N.R., Cai, W.-J., Currie, K., Feely,  
1791 R.A., Sabine, C., Tanhua, T., Tilbrook, B., and Wanninkhof, R.: Advancing best practices for assessing trends  
1792 of ocean acidification time series. *Frontiers in Marine Science*, 9: 1045667. doi: 10.3389/fmars.2022.1045667,  
1793 2022



1794

1795 Takahashi, T., Sutherland, S. C., Wanninkhof, R., Sweeney, C., Feely, R. A., Chipman, D. W., Hales, B.,  
1796 Friederich, G., Chavez, F., Sabine, C., Watson, A. J., Bakker, D. C., Schuster, U., Metzl, N., Yoshikawa-Inoue,  
1797 H., Ishii, M., Midorikawa, T., Nojiri, Y., Körtzinger, A., Steinhoff, T., Hoppema, M., Olafsson, J., Arnarson, T.  
1798 S., Tilbrook, B., Johannessen, T., Olsen, A., Bellerby, R., Wong, C., Delille, B., Bates, N., and de Baar, H. J.:  
1799 Climatological mean and decadal change in surface ocean pCO<sub>2</sub>, and net sea air CO<sub>2</sub> flux over the global  
1800 oceans. *Deep-Sea Res. II*, 56 (8-10), 554–577, <http://dx.doi.org/10.1016/j.dsr2.2008.12.009>. 2009.

1801

1802 Takahashi, T., Sutherland, S. C., Chipman, D. W., Goddard, J. G., Ho, C., Newberger, T., Sweeney, C. and  
1803 Munro, D. R.: Climatological distributions of pH, pCO<sub>2</sub>, total CO<sub>2</sub>, alkalinity, and CaCO<sub>3</sub> saturation in the  
1804 global surface ocean, and temporal changes at selected locations. *Marine Chemistry*, 164, 95–125,  
1805 doi:10.1016/j.marchem.2014.06.004. 2014.

1806

1807 TERNON, J.-F., OUDOT, C., DESSIER, A., DIVERRES, D.: A seasonal tropical sink for atmospheric CO<sub>2</sub> in the Atlantic  
1808 ocean: the role of the Amazon River discharge, *Marine Chemistry*, Volume 68, Issue 3, Pages 183-201,  
1809 [https://doi.org/10.1016/S0304-4203\(99\)00077-8](https://doi.org/10.1016/S0304-4203(99)00077-8), 2000

1810

1811 TESTOR Pierre, COPPOLA Laurent, BOSSE Anthony (2021) MOOSE-GE 2021 cruise, RV Thalassa,  
1812 <https://doi.org/10.17600/18001333>

1813

1814 TESTOR Pierre, COPPOLA Laurent, BOSSE Anthony (2022) MOOSE-GE 2022 cruise, RV Pourquoi pas ?,  
1815 <https://doi.org/10.17600/18001854>

1816

1817 TESTOR Pierre, DURRIEU de MADRON Xavier (2023) MOOSE-GE 2023 cruise, RV Thalassa,  
1818 <https://doi.org/10.17600/18002686>

1819

1820 Thomas, H., Prowe, A. E. F., Lima, I. D., Doney, S. C., Wanninkhof, R., Greatbatch, R. J., Schuster, U. and  
1821 Corbière, A.: Changes in the North Atlantic Oscillation influence CO<sub>2</sub> uptake in the North Atlantic over the past  
1822 2 decades, *Global Biogeochemical Cycles*, 22(4), doi:10.1029/2007GB003167, 2008

1823

1824 Tilbrook, B., Jewett, E. B., DeGrandpre, M. D., Hernandez-Ayon, J. M., Feely, R. A., Gledhill, D. K., Hansson,  
1825 L., Isensee, K., Kurz, M. L., Newton, J. A., Siedlecki, S. A., Chai, F., Dupont, S., Graco, M., Calvo, E., Greeley,  
1826 D., Kapsenberg, L., Lebec, M., Pelejero, C., Schoo, K. L., and Telszewski, M.: An Enhanced Ocean  
1827 Acidification Observing Network: From People to Technology to Data Synthesis and Information Exchange.  
1828 *Frontiers in Marine Science*, 6, 337, DOI:10.3389/fmars.2019.00337, 2019.

1829

1830 TOURATIER Franck, POISSON Alain (1990) MINERVE, <https://doi.org/10.18142/128>

1831

1832 Touratier, F., and Goyet, C.: Decadal evolution of anthropogenic CO<sub>2</sub> in the north western Mediterranean Sea  
1833 from the mid-1990's to the mid-2000's. *Deep Sea Research Part I*.doi:10.1016/j.dsr.2009.05.015, 2009.

1834

1835 Ulses, C., Estournel, C., Fourier, M., Coppola, L., Kessouri, F., Lefèvre, D., and Marsaleix, P.: Oxygen budget  
1836 of the north-western Mediterranean deep- convection region, *Biogeosciences*, 18, 937–960,  
1837 <https://doi.org/10.5194/bg-18-937-2021>, 2021.

1838

1839 Ulses, C., Estournel, C., Marsaleix, P., Soetaert, K., Fourier, M., Coppola, L., Lefèvre, D., Touratier, F., Goyet,  
1840 C., Guglielmi, V., Kessouri, F., Testor, P., and Durrieu de Madron, X.: Seasonal dynamics and annual budget of  
1841 dissolved inorganic carbon in the northwestern Mediterranean deep-convection region, *Biogeosciences*, 20,  
1842 4683–4710, <https://doi.org/10.5194/bg-20-4683-2023>, 2023.

1843

1844 UNESCO: Intercomparison of total alkalinity and total inorganic carbon determinations in seawater. UNESCO  
1845 Tech. Pap. Mar. Sci. 59., 1990

1846

1847 UNESCO: Reference materials for oceanic carbon dioxide measurements. UNESCO Tech. Pap. Mar. Sci. 60.,  
1848 1991  
1849  
1850 United Nations. The Sustainable Development Goals 2020, 68pp. <https://unstats.un.org/sdgs/report/2020/>, 2020  
1851  
1852 Vance, J. M., Currie, K., Suanda, S. H. and Law, C. S.: Drivers of seasonal to decadal mixed layer carbon cycle  
1853 variability in subantarctic water in the Munida Time Series. *Front. Mar. Sci.* 11:1309560. doi:  
1854 10.3389/fmars.2024.1309560, 2024  
1855  
1856 VERNEY Romaric, RABOUILLE Christophe (2012) MERMEX-ACCESS cruise, RV Téthys II,  
1857 <https://doi.org/10.17600/12450070>  
1858  
1859 VIVIER Frédéric, WAELBROECK Claire, MICHEL Elisabeth (2016) NEXT STEP,  
1860 <https://doi.org/10.18142/338>  
1861  
1862 VERNEY Romaric, RABOUILLE Christophe (2012) MERMEX-ACCESS cruise, RV Téthys II,  
1863 <https://doi.org/10.17600/12450070>  
1864  
1865 von Schuckmann, K., Minière, A., Gues, F., Cuesta-Valero, F. J., Kirchengast, G., Adusumilli, S., Straneo, F.,  
1866 Ablain, M., Allan, R. P., Barker, P. M., Beltrami, H., Blazquez, A., Boyer, T., Cheng, L., Church, J.,  
1867 Desbruyeres, D., Dolman, H., Domingues, C. M., García-García, A., Giglio, D., Gilson, J. E., Gorfer, M.,  
1868 Haimberger, L., Hakuba, M. Z., Hendricks, S., Hosoda, S., Johnson, G. C., Killick, R., King, B., Kolodziejczyk,  
1869 N., Korosov, A., Krinner, G., Kuusela, M., Landerer, F. W., Langer, M., Lavergne, T., Lawrence, I., Li, Y.,  
1870 Lyman, J., Marti, F., Marzeion, B., Mayer, M., MacDougall, A. H., McDougall, T., Monselesan, D. P., Nitzbon,  
1871 J., Ootosaka, I., Peng, J., Purkey, S., Roemmich, D., Sato, K., Sato, K., Savita, A., Schweiger, A., Shepherd, A.,  
1872 Seneviratne, S. I., Simons, L., Slater, D. A., Slater, T., Steiner, A. K., Suga, T., Szekely, T., Thiery, W.,  
1873 Timmermans, M.-L., Vanderkelen, I., Wjiffels, S. E., Wu, T., and Zemp, M.: Heat stored in the Earth system  
1874 1960–2020: where does the energy go?, *Earth Syst. Sci. Data*, 15, 1675–1709, [https://doi.org/10.5194/essd-15-](https://doi.org/10.5194/essd-15-1675-2023)  
1875 [1675-2023](https://doi.org/10.5194/essd-15-1675-2023), 2023.  
1876  
1877 Wagener, T., Metzl, N., Caffin, M., Fin, J., Helias Nunige, S., Lefevre, D., Lo Monaco, C., Rougier, G., and  
1878 Moutin, T.: Carbonate system distribution, anthropogenic carbon and acidification in the western tropical South  
1879 Pacific (OUTPACE 2015 transect), *Biogeosciences*, 15, 5221-5236, <https://doi.org/10.5194/bg-15-5221-2018>,  
1880 2018.  
1881  
1882 Wimart-Rousseau, C.: Dynamiques saisonnière et pluriannuelle du système des carbonates dans les eaux de  
1883 surface en mer Méditerranée, *Sciences de l'environnement*. Aix-Marseille Université, [https://hal.archives-](https://hal.archives-ouvertes.fr/tel-03523187)  
1884 [ouvertes.fr/tel-03523187](https://hal.archives-ouvertes.fr/tel-03523187), 2021  
1885  
1886 Wimart-Rousseau, C., Lajaunie-Salla, K., Marrec, P., Wagener, T., Raimbault, P., Lagadec, V., Lafont, M.,  
1887 Garcia, N., Diaz, F., Pinazo, C., Yohia, C., Garcia, F., Xueref-Remy, I., Blanc, P.-E., Armengaud, A., and  
1888 Lefèvre, D.: Temporal variability of the carbonate system and air-sea CO<sub>2</sub> exchanges in a Mediterranean human-  
1889 impacted coastal site. *Estuarine, Coastal and Shelf Science*. <https://doi.org/10.1016/j.ecss.2020.106641>, 2020.  
1890  
1891 Wimart-Rousseau, C., Wagener, T., Álvarez, M., Moutin, T., Fourrier, M., Coppola, L., Niclas-Chirurgien, L.,  
1892 Raimbault, P., D'Ortenzio, F., Durrieu de Madron, X., Taillandier, V., Dumas, F., Conan, P., Pujo-Pay, M. and  
1893 Lefèvre, D.: Seasonal and Interannual Variability of the CO<sub>2</sub> System in the Eastern Mediterranean Sea: A Case  
1894 Study in the North Western Levantine Basin. *Front. Mar. Sci.* 8:649246. doi: 10.3389/fmars.2021.649246, 2021  
1895  
1896 Wimart-Rousseau, C., Wagener, T., Bosse, A., Raimbault, P., Coppola, L., Fourrier, M., Ulses, C. and Lefèvre,  
1897 D.: Assessing seasonal and interannual changes in carbonate chemistry across two timeseries sites in the North  
1898 Western Mediterranean Sea. *Front. Mar. Sci.* 10:1281003. doi: 10.3389/fmars.2023.1281003, 2023.  
1899

1900 WMO/GCOS, 2018: <https://gcos.wmo.int/en/global-climate-indicators>, 2018  
1901  
1902 Yao, M. K., Marcou, O., Goyet, C., Guglielmi, V., Touratier, F., and Savy, J.-P.: Time variability of the north-  
1903 western Mediterranean Sea pH over 1995-2011. *Marine Environmental Research*, doi:  
1904 10.1016/j.marenvres.2016.02.016, 2016  
1905  
1906 Yoder, M. F., Palevsky, H. I., and Fogaren, K. E.: Net community production and inorganic carbon cycling in  
1907 the central Irminger Sea. *Journal of Geophysical Research: Oceans*, 129, e2024JC021027.  
1908 <https://doi.org/10.1029/2024JC021027>, 2024  
1909  
1910 Zhang, S., Wu, Y., Cai, W.-J., Cai, W., Feely, R. A., Wang, Z., et al. : Transport of anthropogenic carbon from  
1911 the Antarctic shelf to deep Southern Ocean triggers acidification. *Global Biogeochemical Cycles*, 37,  
1912 e2023GB007921. <https://doi.org/10.1029/2023GB007921>, 2023  
1913